Force sensation by a Gs-coupled adhesion GPCR mediates equilibrioception by increasing vestibular hair cell membrane excitability and CNGA3 coupling

Zhao Yang[1,4#], Shu-Hua Zhou[1,2,3#], Qi-Yue Zhang[1#], Wen-Wen Liu[5#], Yu Sun[6#], Jie-Yu Qi[2#], Ying Guan[1], Ming-Wei Wang[4,7], Zhi-Chen Song[3], Yu-Nan Sun[8], Wei Yang[9], Xiao Yu[3*], Ren-Jie Chai[2,10*], Jin-Peng Sun[1,4,7,8*]

Affiliations:

[1]Key Laboratory Experimental Teratology of the Ministry of Education, Department of Biochemistry and Molecular Biology, School of Basic Medical Sciences, Cheeloo College of Medicine, Shandong University, Jinan 250012, China.

[2]State Key Laboratory of Digital Medical Engineering, Department of Otolaryngology Head and Neck Surgery, Zhongda Hospital, School of Life Sciences and Technology, Advanced Institute for Life and Health Jiangsu Province High-Tech Key Laboratory for Bio-Medical Research, Southeast University, Nanjing 210096, China.

[3]Key Laboratory of Experimental Teratology of the Ministry of Education, Department of Physiology, School of Basic Medical Sciences, Cheeloo College of Medicine, Shandong University, Jinan 250012, China.

[4]Advanced Medical Research Institute, Cheeloo College of Medicine, Shandong University, Jinan 250012, China.

[5]Department of Otolaryngology-Head and Neck Surgery, Shandong Provincial ENT Hospital, Cheeloo College of Medicine, Shandong University, Jinan, 250014, China.

[6]Department of Otorhinolaryngology, Union Hospital, Tongji Medical College, Huazhong University of Science and Technology, Wuhan, China.

[7]Department of Clinical Laboratory, The Second Hospital, Cheeloo College of Medicine, Shandong University, Jinan 250012, China.

[8]Key Laboratory of Molecular Cardiovascular Science of the Ministry of Education, Department of Physiology and Pathophysiology, School of Basic Medical Sciences, Peking University, Beijing 100191, China.

[9]Department of Biophysics, and Department of Neurology of the Fourth Affiliated Hospital,

Zhejiang University School of Medicine, Hangzhou 310058, China.
[10]Co-Innovation Center of Neuroregeneration, Nantong University, Nantong 226001, China.
# These authors contributed equally to this work.
* Correspondence: Jin-Peng Sun, E-mail: sunjinpeng@sdu.edu.cn
Ren-Jie Chai, E-mail: renjiec@seu.edu.cn
Xiao Yu, E-mail: yuxiao@sdu.edu.cn

Abstract

Equilibrioception is essential for the perception and navigation of mammals in the three-dimensional world. The mechanoelectrical transduction (MET) process in vestibular hair cells is believed to play central roles in positional and motional sensation. However, the direct equilibrioception sensor at the molecular level is not clear, and the mechanism underlying the MET process in vestibular hair cells remains elusive. Here, we identified that the G protein-coupled receptor LPHN2, which is expressed in the cuticular plate of utricular hair cells, is required for normal balance maintenance. The sensation of force by LPHN2 in the utricular hair cells increased intracellular cAMP levels in a Gs-dependent manner. The direct association of LPHN2 with the ion channel CNGA3 and increased cAMP levels enabled the activation of CNGA3, which induced calcium influx and membrane depolarization. These cellular signals and balance-related functions were significantly weakened in *Lphn2*$^{+/-}$ mice, *Pou4f3-CreER*$^{+/-}$ *Lphn2*$^{fl/fl}$ mice and *Pou4f3-CreER*$^{+/-}$*Cnga3*$^{fl/+}$ mice and could be suppressed by Gs or CNGA3 inhibitors. Collectively, our data suggested that LPHN2 could be a direct equilibrioception sensor in utricular hair cells by converting the force sensation to electrical signals through Gs and CNGA3 coupling. Both GPCR members and the ion channel CNGA3 could be essential elements for equilibrioception.

Introduction

The sense of balance and motion enables our perception and navigation in the three-dimensional world and is thus critical to our interactions with the world. The positional or motional information is primarily perceived by the hair cells located in the sensory epithelium of the vestibular end organs, which include two perpendicularly arranged otolith organs, the

utricle and saccule, and three semicircular canals[1,2]. Vestibular hair cells transmit balance information about head motion or tilt through a mechanoelectrical transduction (MET) process that converts mechanical force into electrical signals. The MET process is thought to be mainly regulated by mechanotransduction ion channels, with the mechanism remaining largely elusive[3,4]. In addition to ion channels, recent studies have also uncovered a regulatory role of G protein-coupled receptors (GPCRs) in the vestibular system[5,6]. For example, CELSR1 regulates vestibular functions by coordinating the planar polarity of hair cells, and CELSR1 deficiency in mice leads to balance dysfunction[7]. However, it is still unknown whether GPCRs directly regulate the mechanotransduction in balance sensation.

In our parallel study described in a companion paper, which was started three years earlier than the current manuscript, we identified 5 receptors, including GPR133, GPR126, LPHN2, LPHN3 and VLGR1, as mechanosensitive GPCRs in the utricle by screening the mechanosensitive potential of GPCRs in utricular hair cells using a combination of cellular assays and an animal model of balance dysfunction. Importantly, we identified that GPR133 converts mechanical stimuli into intracellular cAMP signals in utricular hair cells through Gi engagement, which suppress MET and inhibits plasma membrane excitability. This work suggests a potential of GPCR-Gi signalling-modulated inhibition of membrane excitability in equilibrioception, which appears similar to the events that occur during vision sensation[8]. However, whether a positive modulation of vestibular membrane excitability by GPCR-mediated MET, a process similar to those in odour and taste sensation[9,10], is involved in the activation of Gs signalling remains unclear (Figure 1A).

Notably, of the 5 mechanosensitive GPCRs in the utricle, LPHN2 and VLGR1 activate Gs signalling in response to force stimulation. Therefore, in the present study, we further explored the potential role of Gs signalling of mechanosensitive GPCRs in equilibrioception using LPHN2 as the representative receptor since VLGR1 knockout did not result in significant balance phenotypes. We found that LPHN2 specifically expressed in the cuticular plate of utricular hair cells is indispensable for equilibrioception. Global knockout or hair cell-specific knockout of *Lphn2* in mice impairs balance. Mechanistically, force sensation by LPHN2 promotes an increase in the cAMP levels of utricular hair cells, which activates CNGA3 channels and induces membrane depolarization. Consistently, inhibiting CNGA3 activity by

91 pharmacological or genetic approaches eliminates LPHN2-mediated MET, leading to balance
92 dysfunction. Therefore, our study identifies an equilibrioception-regulating GPCR that
93 participates in MET by activating Gs-cAMP signalling.
94
95 **Results**
96 **Mechanosensitive LPHN2 is essential for normal vestibular functions**
97 Quantitative RT–PCR (qPCR) analysis of LPHN expression from mouse utricles harvested
98 at different time points revealed that all three LPHN subfamily members (LPHN1-3) showed
99 constant and stable expression from late embryo (E15) to adulthood (P120) (Figure S1A). Both
100 single-cell RNA sequencing (scRNA-seq) data and the results from our single-hair-cell qRT–
101 PCR analysis indicated that all three LPHNs were expressed in the utricular hair cells of mice,
102 ranging from 57% to 95% for expression frequency[11] (Figures 1B and S1B). Compared with
103 that of LPHN1, the average expression levels of LPHN2 and LPHN3 were relatively higher,
104 approximately 6- and 3-fold, respectively (Figures 1C and S1C). We next examined the
105 mechanosensitive property of LPHNs using a magnetic force stimulation system in which
106 magnetic force was applied to paramagnetic beads coated with anti-Flag antibody (referred to
107 as Flag-M-beads) and interacted with N-terminal Flag-tagged LPHNs expressed in HEK293
108 cells (Figure S1D). The force-induced activation of LPHNs was determined by inspecting the
109 downstream dissociation of G protein heterotrimers as revealed by a bioluminescence
110 resonance energy transfer (BRET) assay. All three LPHNs showed significant Gi activity in
111 response to 3 pN force stimulation (Figure 1D). Notably, only LPHN2, but not LPHN1 or
112 LPHN3, displayed detectable force-stimulated Gs activity (Figures 1E and S1E). The higher
113 expression levels of LPHN2 and LPHN3 in the murine utricular hair cells compared with that
114 of LPHN1 and their mechanosensitive capability collectively prompted us to explore the
115 potential vestibular functions of these two receptors.
116 Initially, heterozygous *Lphn2* and *Lphn3* gene knockout KO mice were used for
117 equilibration-related phenotype analysis since constitutive KO of *Lphn2* or *Lphn3* caused
118 embryonic lethality and developmental defects, respectively[12,13]. The deficiency of one copy of
119 LPHN2 or LPHN3 in the heterozygous KO mice was verified by genotyping PCR and western
120 blotting analysis (Figures S2A-S2H). These mice were viable and had body weights

121 comparable to those of their WT littermates (Figure S2I). The vestibular behaviours of the mice
122 at P40 were assessed through the rotarod test and forced swimming test. Despite their nearly
123 normal performance in the rotarod test (*Lphn2*$^{+/-}$ 109.5 ± 6.43 s vs. WT 106.2 ± 5.36 s), the
124 *Lphn2*$^{+/-}$ mice showed impaired performance in the open field test, displaying significantly
125 elevated circulating and travelling activities in both 2 min and 10 min time frames (Figures 1F-
126 1H). Moreover, compared with their WT littermates, the *Lphn2*$^{+/-}$ mice showed impaired
127 swimming ability, with a swimming score of 0.88± 0.13 (the 0–3 scoring system was used, and
128 WT mice had scores of 0) (Figure 1I). In contrast, compared with the WT mice, the *Lphn3*$^{+/-}$
129 mice showed no significant difference in the open field test, rotarod test or forced swimming
130 tests (Figures 1F-1I).
131 To further investigate the vestibular functions of these heterozygous LPHN-deficient mice,
132 we measured the vestibular-ocular reflex (VOR) responses of the mice to sinusoidal head
133 rotations at P40. Notably, compared with the WT mice, the *Lphn2*$^{+/-}$ mice showed an
134 approximately 25%-50% decrease in compensatory VOR gains in response to either earth-
135 vertical or off-vertical axis rotation, suggesting a deficiency in both the semicircular canals and
136 otolith system (Figures 1J-1M). In contrast, the *Lphn3*$^{+/-}$ mice showed normal eye movement
137 responses in both VOR tests (Figures 1J-M). Collectively, these results indicated that LPHN2
138 but not LPHN3 plays an important role in balance maintenance.
139
140 **Expression pattern of LPHN2 in utricular hair cells**
141 We next examined the expression patterns of LPHN2 in the mouse utricle by whole-mount
142 immunostaining, which showed specific expression in approximately 80% of myo7a-positive
143 hair cells (Figures 2A and S3A). The specificity of the LPHN2 antibody was supported by both
144 western blotting results in HEK293 cells expressing different LPHNs and immunostaining of
145 utricles derived from *Lphn2*$^{-/-}$ mice at E18 (*Lphn2*$^{-/-}$ mice showed embryonic lethality) (Figures
146 2A and S3B). The expression pattern of LPHN2 was further supported by RNAscope in situ
147 hybridization, which revealed a comparable LPHN2-expressing hair cell proportion (~80%) to
148 that inspected by immunostaining (Figures 2B and 2C). To further determine the subcellular
149 localization of LPHN2 in utricular hair cells, we examined the expression pattern of LPHN2 in
150 different optical sections spanning from the stereocilia to the hair cell body. LPHN2 expression

151 was detected only at the apical surface of the hair cells, as revealed by its coimmunostaining
152 with spectrin, which is a specific marker of the cuticular plate in hair cells[14,15] (Figures 2D and
153 S3C). In contrast, LPHN2 expression was not detected within the stereocilia or along the
154 basolateral membrane of hair cells (Figure 2D). The specific expression of LPHN2 at the
155 cuticular plate was further supported by section staining of the utricle sensory epithelium using
156 MYO7A and SOX2 as the hair cell and supporting cell markers, respectively (Figure 2E). The
157 unique expression pattern of mechanosensitive LPHN2 in the utricular hair cells suggests that
158 it might participate in the interactions between the hair cells and the otoconial matrix, which
159 play important roles in force sensation.
160

161 **LPHN2 in vestibular hair cells specifically regulates balance sensation**

162 To assess the specific functional role of LPHN2 in vestibular hair cells, we crossed *Lphn2*$^{fl/fl}$
163 mice with inducible *Pou4f3-CreER*$^{+/-}$ transgenic mice (Figure 3A). Pou4f3 is the transcriptional
164 target of ATOH1 and a commonly used marker of hair cells, which is expressed in all LPHN2-
165 positive utricular hair cells, as revealed by scRNA-seq data[11,16] (Figures S3D and S3E). The
166 specificity of LPHN2 ablation in the vestibule of *Pou4f3-CreER*$^{+/-}$*Lphn2*$^{fl/fl}$ mice was indicated
167 by the loss of LPHN2 immunostaining in Pou4f3-expressing utricular hair cells but not in other
168 tissues, such as the brainstem (Figures 3B and S3F). The specific elimination of Lphn2
169 expression in the vestibule of *Pou4f3-CreER*$^{+/-}$*Lphn2*$^{fl/fl}$ mice was further supported by western
170 blotting analysis (Figure S3G).

171 A battery of behavioural tests was conducted to assess the effects of LPHN2 ablation in
172 vestibular hair cells on balance maintenance. Notably, in addition to their significantly declined
173 swimming performance, the *Pou4f3-CreER*$^{+/-}$*Lphn2*$^{fl/fl}$ mice showed approximately 50%
174 shorter durations in the rotarod test than their *Pou4f3-CreER*$^{+/-}$*Lphn2*$^{+/+}$ littermates, which was
175 not observed in the *Lphn2*$^{+/-}$ mice (Figures 3C and 3D). Moreover, compared with their *Pou4f3-*
176 *CreER*$^{+/-}$*Lphn2*$^{+/+}$ littermates, the *Pou4f3-CreER*$^{+/-}$*Lphn2*$^{fl/fl}$ mice exhibited an approximately
177 2-fold increase in circling times in both the 2 min and 10 min testing time frames, accompanied
178 by significantly increased travelling distances (Figures 3E,3F and S3H). Furthermore,
179 compared with littermate control mice, *Pou4f3-CreER*$^{+/-}$*Lphn2*$^{fl/fl}$ mice showed an
180 approximately 25%~50% decrease in the VOR response in either the earth-vertical or off-

181 vertical axis rotation test (Figures 3G and 3H). Collectively, these results suggest a balance-
182 regulatory role of LPHN2 in vestibular hair cells.
183
184 **Force sensing by LPHN2 increases the cAMP levels of utricular hair cells**
185 Downstream of GPCR activation, changes in the intracellular levels of second messengers,
186 such as cAMP and Ca^{2+}, play central roles in the sensation of odour, taste and vision[9,10,17-20]. For
187 instance, the sensation of odour by olfactory receptors triggers the cAMP signalling cascade
188 that finally results in an influx of Ca^{2+} and excitation of olfactory neurons[9,17]. Detection of the
189 sweet or bitter by taste receptors produced DAG and IP3, followed by the opening of the taste-
190 transduction channel TRPM5[10,21]. Since our G protein activity analysis indicated that the force
191 sensation by LPHN2 was able to activate Gs and Gi, two G protein subtypes modulating
192 intracellular cAMP levels, we measured the changes in cAMP levels downstream of LPHN2 in
193 the utricle explant using paramagnetic beads coated with anti-LPHN2 antibody (referred to as
194 LPHN2-M-beads), which recognizes the N-terminal residues 551-600 of LPHN2. In the
195 heterologous system, we showed that upon magnetic force application, the LPHN2-M-beads
196 induced dose-dependent cAMP accumulation in LPHN2-overexpressing HEK293 cells but not
197 in cells transfected with the empty vector pcDNA3.1 (Figures 4A and S4A). The EC50 for the
198 LPHN2-M-bead-induced cAMP level increase in vitro was 1.70± 0.34 pN. In contrast, the
199 polylysine-coated paramagnetic beads (Ctrl-beads) could not induce cAMP production in
200 LPHN2-expressing HEK293 cells in response to force application, thus supporting the
201 specificity of the LPHN2-M-bead in activating LPHN2 (Figure 4A). We subsequently applied
202 the LPHN2-M-bead to the murine utricle explant and revealed that the administration of
203 magnetic force to the beads dose-dependently increased the intracellular cAMP level from
204 approximately 4.4 mM to 6.4 mM in the *Pou4f3-CreER*$^{+/-}$*Lphn2*$^{+/+}$ utricle explant (with an
205 EC50 of 1.64 ± 0.13 pN) but not in the *Pou4f3-CreER*$^{+/-}$*Lphn2*$^{fl/fl}$ utricle explant, using the
206 adenylyl cyclase activator forskolin as the positive control (Figures 4B and S4B). In contrast,
207 the endogenous cAMP levels in the utricle explants were not significantly affected by force
208 application via Ctrl-beads (Figure 4B). These results indicated that Gs-cAMP signalling
209 downstream of LPHN2 was activated in utricular hair cells in response to force stimulation.
210 Consistently, the expression profiling of isolated utricular hair cells by single-cell qRT–PCR

211 revealed that Gs is the most abundantly expressed G protein subtype in 15 tested LPHN2-
212 positive cells (Figures 4C and 4D). Moreover, the force stimulation activated the Gs pathway
213 of LPHN2 in the heterologous system with an EC50 of 1.75 ± 0.02 pN, which is significantly
214 stronger than the EC50 values of Gi subtype pathways (Gi1: 3.79 ± 0.05 pN, Gi2: 4.61 ±
215 0.09 pN, Gi3: 3.52 ± 0.09 pN) (Figures 4E-4G and S4C-S4D). In contrast, the mechanical force
216 applied by LPHN2-M-beads did not activate the Go or G12 pathway downstream of LPHN2
217 (Figures S4E and S4F).
218

219 **Force sensing by LPHN2 induces Gs-dependent Ca^{2+} influx in utricular hair cells**

220 Intracellular Ca^{2+} is a key element for neurotransmitter release and may play a pivotal role in
221 equilibration sensation[21-24]. We next examined the Ca^{2+} response downstream of LPHN2 in
222 single hair cells after force stimulation. The AAV-ie-*Lphn2pr*-mCherry, in which the original
223 CAG promoter in AAV-ie was replaced with the promoter region (800 bp) of *Lphn2*, was
224 delivered to the P3 mice through round window membrane injection (Figures 4H, S4G and
225 S4H). This modified AAV-ie-*Lphn2pr*-mCherry enabled mCherry expression specifically in
226 LPHN2-expressing utricular hair cells, which was supported by immunofluorescence and
227 single-cell RT–PCR (Figure S4I). The Ca^{2+} signal in LPHN2-expressing utricular hair cells in
228 response to force stimulation was recorded by a Fura-2 fluorescent probe. Approximately 35%
229 of the LPHN2-expressing hair cells derived from the *Pou4f3-CreER*$^{+/-}$*Lphn2*$^{+/+}$ utricle showed
230 an increase in Ca^{2+} levels in response to force stimulation (Figures 4I-4K). In contrast, the AAV-
231 ie-*Lphn2pr*-mCherry-labelled utricular hair cells derived from *Pou4f3-CreER*$^{+/-}$*Lphn2*$^{fl/fl}$ mice
232 showed no detectable Ca^{2+} signals in response to force application via LPHN2-M-beads
233 (Figures 4I-4K and S4J). Importantly, the force-stimulated Ca^{2+} response in LPHN2-expressing
234 hair cells was completely abolished by pre-treatment with the Gs inhibitor NF-449 but was not
235 affected by the PKA inhibitor PKI 14-22 or the Gq inhibitor YM-254890 (Figure 4J). These
236 results suggested that the force-induced Ca^{2+} response was Gs-dependent and Gq-independent.
237 Consistent with this hypothesis, force stimulation of LPHN2 did not induce detectable
238 production of IP3, the messenger molecule downstream of the Gq pathway, in utricular hair
239 cells (Figure 4M). Moreover, the force-induced Ca^{2+} response in LPHN2-expressing hair cells
240 was abolished when the utricle explants were incubated in Ca^{2+}-free buffer (Figure 4N).

241 Collectively, these results suggested that the activation of LPHN2 by force stimulation induced
242 Gs-dependent Ca^{2+} influx in utricular hair cells, which was most likely regulated by an
243 unknown cation channel.
244
245 **LPHN2 activation by force elicits membrane depolarization in utricular hair cells**
246 The force-induced Ca^{2+} influx in utricular hair cells through activating LPHN2 suggested
247 that an unknown downstream ion channel localized in the hair cell was open and might cause
248 membrane potential changes. Therefore, we examined the excitability of the utricular hair cells
249 in response to force activation of LPHN2 via LPHN2-M-beads by whole-cell patch-clamp
250 recording. We found that approximately 32% of LPHN2-expressing hair cells (labelled with
251 AAV-ie-*Lphn2pr*-mCherry) in *Pou4f3-CreER*$^{+/-}$*Lphn2*$^{+/+}$ utricle explants showed an
252 approximately 50% increase in current amplitude in response to 3 pN force stimulation (17 out
253 of 53, cluster I), whereas the other 68% were force insensitive (36 out of 53, cluster II) (Figures
254 5A-5C). In general, cluster I cells had a higher maximum current amplitude than cluster II cells
255 by approximately 1.7-fold at a holding potential of 100 mV (Figure S5A). The proportion of
256 force-sensitive utricular hair cells was in accordance with that recorded in the force-stimulated
257 calcium response assay (Figure 4K). As the negative control, AAV-ie-*Lphn2pr*-mCherry-
258 labelled hair cells in utricle explants derived from *Pou4f3-CreER*$^{+/-}$*Lphn2*$^{fl/fl}$ mice showed no
259 detectable electrophysiological response to force stimulation via LPHN2-M-beads (Figures 5A-
260 5C and S5B). Notably, similar to those in their *Pou4f3-CreER*$^{+/-}$*Lphn2*$^{+/+}$ counterparts, the
261 mCherry-labelled utricular hair cells in *Pou4f3-CreER*$^{+/-}$*Lphn2*$^{fl/fl}$ mice could also be divided
262 into two clusters, with cluster I cells (13 out of 39, 33%) showing significantly higher current
263 amplitude than cluster II cells (26 out of 39, 67%) at the same holding potentials (Figures 5A-
264 5B). The recorded currents in cluster I cells were voltage-dependent and showed pronounced
265 outwards rectification, with a reversed potential of approximately -20 mV (Figures 5A-5B).
266 To further explore the functional consequences of force-stimulated LPHN2 in utricular hair
267 cells, we recorded the resting membrane potential of the force-sensitive cluster I cells using a
268 current clamp. When holding at 0 pA, force stimulation with LPHN2-M-beads induced dose-
269 dependent depolarization of the *Pou4f3-CreER*$^{+/-}$*Lphn2*$^{+/+}$ cluster I cells with an EC50 of 1.83
270 ± 0.05 pN (Figures 5D, S5C and S5D), which is similar to that recorded in the Gs protein

activation assay in LPHN2-overexpressing HEK293 cells (Figure 4E). In contrast, the cluster I hair cells from *Pou4f3-CreER*$^{+/-}$*Lphn2*$^{fl/fl}$ mice showed no significant membrane potential changes in response to force stimulation via LPHN2-M-beads (Figure 5D). Notably, the alteration of the hair cell membrane potential was recorded as 704.73 ± 8.99 ms after the force application, which was recovered to the basal level after 3 s of force stimulation (with a time latency of 365.13 ± 10.10 ms after force removal) (Figures 5D and 5E). The response kinetics of the force-induced membrane potential change could be fitted with a monoexponential equation, with a response time constant (τ_p) and a recovery time constant (τ_{rec}) of 253.70 ± 3.78 ms and 250.33 ± 10.15 ms, respectively (Figure 5E). Consistent with the current clamp data, when holding at a potential of +100 mV or -70 mV, the current amplitudes of the cluster I hair cells derived from the *Pou4f3-CreER*$^{+/-}$*Lphn2*$^{+/+}$ utricle explants, but not those from *Pou4f3-CreER*$^{+/-}$*Lphn2*$^{fl/fl}$ utricle explants, were significantly increased in response to force stimulation via LPHN2-M-beads (Figures 5F and S5E). Importantly, both the force-stimulated increase in current and membrane potentials were completely blocked by pre-treatment with the Gs inhibitor NF449 (Figures 5G,5H and S5F). Collectively, these results suggest that force-stimulated LPHN2 activation in utricular hair cells promoted Ca^{2+} influx and membrane depolarization, probably via an unknown cation channel.

LPHN2 regulates mechanoelectrical transduction through coupling to CNGA3

The dependency of LPHN2-mediated calcium influx and membrane depolarization on Gs-cAMP signalling implies that the force sensation of LPHN2 might be converted to electrical signals by activating cAMP-sensitive ion channel(s). Therefore, we analysed the expression pattern of cyclic nucleotide–gated (CNG) channels and hyperpolarization-activated cyclic nucleotide–modulated (HCN) channels, two principle subfamilies of cyclic nucleotide-regulated cation channels that play essential roles in various neuronal activities[25,26], in utricular hair cells. The scRNA-seq data indicated that at least 3 CNG channels (CNGA1, CNGA3 and CNGB1) and 2 HCN channels (HCN1 and HCN4) were found to be expressed in LPHN2-expressing utricular hair cells (Figure 6A). Further qRT–PCR analysis of single utricular hair cells revealed that CNGA3 was specifically expressed in force-sensitive LPHN2-expressing hair cells (cluster I cells), whereas the other channels were almost equally expressed in cluster

301 I and II cells (Figure 6B). Furthermore, only CNGA3, but not the other cyclic nucleotide-
302 regulated channels expressed in LPHN2-expressing utricular hair cells, showed direct
303 association with LPHN2, as revealed by an *in vivo* coimmunoprecipitation assay (Figure 6C).
304 Consistently, a substantial portion of LPHN2 showed coimmunostaining with CNGA3 at the
305 cuticular plate of utricular hair cells, supporting interactions between these two membrane
306 proteins (Figure 6D).

307 Next, we tested whether force-induced activation of LPHN2 was directly coupled with
308 CNGA3 current changes using an in vitro HEK293 overexpression system. Notably, co-
309 expression of CNGA3, but not CNGA1 or HCN1/4 channels, enabled the membrane
310 excitability of the LPHN2-expressing HEK293 cells in response to 3 pN force stimulation
311 applied by LPHN2-M-beads, thus suggesting the importance of the physical association
312 between LPHN2 and CNGA3 channels (Figures 6E and S6A-S6C). At the holding potential of
313 +100 mV, the force induced a dose-dependent increase in current amplitude only in HEK293
314 cells co-expressing LPHN2 and CNGA3, with an EC50 of 1.71 ± 0.01 pN (Figures 6F and
315 S6D). This EC50 value was close to those recorded for the force-induced membrane potential
316 changes or cAMP accumulation via LPHN2-M-beads in utricle explants (Figure 6G).
317 Collectively, these results suggest the direct interaction and functional coupling between
318 CNGA3 and LPHN2 in response to force stimulation.

319

320 **Inhibition of CNGA3 activity severely impairs balance**

321 To further explore the functional importance of CNG channels in balance maintenance, we
322 assessed the effects of the CNG inhibitor L-cis-diltiazem on the equilibration-related
323 behaviours of mice. Notably, intraperitoneal injection of L-cis-diltiazem for 3 consecutive days
324 significantly increased the circling behaviour and travelling distance of mice compared with
325 the control group in both the 2 min time frame (9.75 ±1.0 circles vs. 5.75 ± 0.63 circles) and 10
326 min time frame (30.00 ± 1.68 circles vs. 21.50 ± 1.85 circles) (Figures S7A-S7C). Moreover,
327 L-cis-diltiazem administration significantly deteriorated mouse performance in both forced
328 swimming (swimming scores of 1.50 ± 0.29 vs. 0) and rotarod tests (staying time of 66.70 ±
329 5.34 s vs. 103.54 ± 9.32 s) (Figures S7D and S7E). These data suggested a regulatory role of
330 the CNG channel in vestibular functions.

To exclude the potential nonselectivity of L-cis-diltiazem by inhibiting multiple CNG channel subtypes and to inspect the specific role of CNGA3 in vestibular hair cells, we generated a hair cell-specific *Cnga3*-knockout mouse line by crossing *Cnga3*$^{fl/fl}$ mice with *Pou4f3-CreER*$^{+/-}$ transgenic mice (Figures S7F and S7G). The specific knockdown (approximately 50%) of CNGA3 expression in the vestibule of *Pou4f3-CreER*$^{+/-}$*Cnga3*$^{fl/+}$ mice was verified by both western blotting (Figures S7H and S7I). In contrast, the CNGA3 expression levels in other tissues, such as the brainstem and skin, were not significantly affected (Figures S7H and S7I). Importantly, compared with their *Pou4f3-CreER*$^{+/-}$*Cnga3*$^{+/+}$ littermates, the *Pou4f3-CreER*$^{+/-}$*Cnga3*$^{fl/+}$ mice showed significantly impaired balance behaviours, including increased circling and travelling distance, reduced duration time on the rotarod and deteriorated swimming performance (Figures 7A-7E). Moreover, the *Pou4f3-CreER*$^{+/-}$*Cnga3*$^{fl/+}$ mice showed a more than 80% reduction in VOR gain in off-vertical axis rotation (otolith function test) and a 25%-40% reduction in VOR responses to earth-vertical axis rotation (semicircular canal function test) (Figures 7F-7H). These results collectively indicated a critical role of CNGA3 channels, especially those expressed in otolith organs, in normal balance maintenance. These channels most likely act as a key signalling component downstream of force-sensing LPHN2 and directly converts the chemical signals delivered by second messengers into electrical signals. Consistent with this hypothesis, the application of 100 μM L-cis-diltiazem in cluster I utricular hair cells completely abolished the force-stimulated calcium signals or current amplitude change after the activation of LPHN2 by LPHN2-M-beads (Figures 7I-7K). In other words, inhibition of CNGA3 activity eliminated the force sensitivity of LPHN2-expressing utricular hair cells and turned all of the LPHN2-expressing cells into cluster II cells (Figures S7J and S7K). Altogether, these results suggest that an LPHN2-CNGA3 functional axis modulates the membrane excitability of utricular hair cells in response to force sensation, which contributes to equilibrioception.

Notably, CNGA3 expression is not confined to the cuticular plate of utricular hair cells where it colocalizes with LPHN2 but is also observed at the lateral and basal membranes (Figure 6D). Therefore, we speculated that CNGA3 might also regulate utricular hair cell functions through other pathways or connect with other GPCRs, in addition to its crosstalk with LPHN2. This notion might explain the aggravated phenotypes of *Cnga3*-deficient mice in balance behaviour

361 tests compared with those of *Lphn2*-deficient mice.

362

363 **Re-expression of LPHN2 in vestibular hair cells rescued the equilibrioception of LPHN2-**
364 **deficient mice**

365 To further inspect the functional roles of LPHN2 specifically expressed in the vestibular
366 system, we reintroduced LPHN2 expression in utricular hair cells of *Pou4f3-CreER*$^{+/-}$*Lphn2*$^{fl/fl}$
367 mice via AAV delivery. Our previous structural and functional analyses revealed that the force
368 sensation by adhesion GPCRs was primarily mediated by the juxtamembrane GAIN domain[27,28].
369 Consistently, the Flag-tagged LPHN2-GAIN construct with the deletion of 523 N-terminal
370 residues retained mechanosensitive potential and showed dose-dependent Gs signalling in
371 response to force stimulation with Flag-M-beads, and the response was comparable to that of
372 full-length LPHN2 when expressed at similar levels (Figures S8A and S8B). Therefore, we
373 packaged the Flag-LPHN2-GAIN sequences into the AAV-ie-*Lphn2pr*-mCherry vector
374 (mCherry following an IRES element was fused to the C-terminus of LPHN2-GAIN, referred
375 to as AAV-ie-LPHN2) and delivered the virus into P3 *Pou4f3-CreER*$^{+/-}$*Lphn2*$^{fl/fl}$ mice through
376 round window membrane injection using AAV-ie-*Lphn2pr*-mCherry as a negative control
377 (Figure S8C). The specific expression of LPHN2-GAIN in the utricular hair cells, but not in
378 the brains, of *Pou4f3-CreER*$^{+/-}$*Lphn2*$^{fl/fl}$ mice was observed 14 days after the administration of
379 AAV-ie-LPHN2 using western blotting and immunofluorescence (Figures S8D and S8E). As a
380 negative control, *Pou4f3-CreER*$^{+/-}$*Lphn2*$^{fl/fl}$ mice infected with AAV-ie-*Lphn2pr*-mCherry
381 revealed only specific utricular hair cell labelling but no detectable LPHN2-GAIN expression
382 (Figures S8D and S8E).

383 We next assessed the equilibration-related behaviours of mice receiving LPHN2-GAIN gene
384 delivery. Notably, the LPHN2-deficient mice treated with AAV-ie-LPHN2 showed significantly
385 improved performance in all behaviour studies related to equilibrioception, including the forced
386 swimming, open field and rotarod tests, and the performances were comparable to those of the
387 WT mice (Figures 8A-8D). Moreover, the VOR gain values of AAV-ie-LPHN2-treated *Pou4f3-*
388 *CreER*$^{+/-}$*Lphn2*$^{fl/fl}$ mice at all tested frequencies in both the earth-vertical and off-vertical axis
389 rotation tests recovered to levels comparable to those of WT mice (Figures 8E and 8F). As a
390 negative control, LPHN2-deficient mice treated with AAV-ie-*Lphn2pr*-mCherry showed no

391 significant improvement in any of the above tests (Figures 8A-8F). Furthermore, compared
392 with the mCherry-labelled utricular hair cells in control virus-treated *Pou4f3-CreER*$^{+/-}$*Lphn2*$^{fl/fl}$
393 mice, which showed no Ca^{2+} response or current amplitude changes to Flag-M-bead-induced
394 force stimulation, approximately 31% and 30% of the labelled utricular hair cells in AAV-ie-
395 LPHN2-treated *Pou4f3-CreER*$^{+/-}$*Lphn2*$^{fl/fl}$ mice regained force-induced excitability, resembling
396 that observed for WT utricle cluster I hair cells (Figures 8G, S8F and S8G). Therefore,
397 reintroduction of the mechanosensitive LPHN2-GAIN specifically in *Lphn2* promoter-labelled
398 utricular hair cells was able to rescue the equilibrioception of LPHN2-deficient mice. These
399 findings further supported that force-activated LPHN2 in the vestibular system directly
400 contributes to normal equilibrioception.
401
402 **Discussion**
403 Despite its importance for our daily living and motion in three-dimensional space, the
404 molecular mechanism underlying the sense of balance remains elusive. Previous studies have
405 revealed that ion channels, such as TMC1/2, are potential key components of the MET process,
406 which is essential for equilibrioception[29-31]. However, direct evidence for force sensation by
407 TMC1/2 is lacking, and the direct force sensors that participate in equilibrioception are not clear.
408 In addition to ion channels, another group of membrane receptors, GPCRs, are known as direct
409 sensors for vision, odour and touch[8,32,33]. Although recent studies have identified that the GPCR
410 member CELSR is essential for equilibrioception by modulating the planar polarity of hair
411 cells[7], whether GPCRs, especially those with mechanosensitive potentials, directly participate
412 in the MET process of equilibrioception remains unclear. In our parallel work, which we started
413 three years earlier than the present manuscript, we found that the mechanosensitive GPCR
414 GPR133 participates in MET and is indispensable for balance maintenance in mice. Here, we
415 identified that another mechanosensitive GPCR, LPHN2, is also able to sense force in
416 vestibular hair cells to mediate MET and is essential for equilibrioception. These two parallel
417 works support the likely existence of multiple GPCRs that function as force sensors and MET
418 mediators essential for equilibrioception, although further exploration is needed to confirm this
419 hypothesis.
420 In our study, heterozygous *Lphn2*-deficient mice showed reduced balance performance and

421 impaired VOR, which were further deteriorated in mice with hair cell-specific ablation of
422 LPHN2 in an inducible manner. Importantly, specific re-expression of LPHN2 in vestibular hair
423 cells rescued the equilibrioception of *Pou4f3-CreER*$^{+/-}$*Lphn2*$^{fl/fl}$ mice. These data collectively
424 support the notion that mechanosensitive LPHN2 is at least a part of the balance-sensing
425 machinery in peripheral vestibular end organs. Intriguingly, LPHN2 is specifically expressed
426 at the cuticular plate of utricular hair cells, which is similar to the expression pattern of the
427 mechanotransduction channel PIEZO2[34]. Therefore, we speculated that the MET process is not
428 confined to hair cell stereocilia and that mechanosensitive GPCRs and/or channels at the apical
429 surface might also play important roles in the MET process through direct mechanical force
430 sensation or interaction with the extracellular or otoconial matrix.

431 Notably, GPCRs play important roles in the sensation of vision, olfaction and three taste
432 qualities (sweet, bitter and umami) by modulating the intracellular levels of second messengers.
433 For instance, the sensation of vision by rhodopsin relies on the Gt-mediated reduction of cGMP
434 levels in photoreceptor cells, and the perception of odour by odourant receptors depends on the
435 G_{olf}-regulated accumulation of cAMP in olfactory neurons[19,35]. In a parallel paper, we showed
436 that GPR133 decreased the basal cAMP levels of vestibular hair cells in a Gi-dependent manner
437 after force stimulation. We speculated that the inhibitory effect of the mechanosensitive
438 GPR133 on intracellular cAMP levels might resemble the regulatory processes that occur
439 during vision sensation. In contrast, our present work indicated that LPHN2 could promote
440 MET in utricular hair cells by activating Gs-cAMP signalling, demonstrating a positive
441 modulation of vestibular membrane excitability. This special GPCR-mediated positive MET
442 resembles the signalling mechanisms for olfaction and sweet/bitter taste perception. Therefore,
443 we speculated that the force sensation mediated by LPHN2 and GPR133, as well as potentially
444 other GPCRs, in vestibular hair cells might encode combinatory positional information. For a
445 simplified model, we hypothesized that a given force applied to hair cells with different
446 expression patterns of these two receptors (LPHN2^{+}GPR133^{+}, LPHN2^{+}GPR133^{-}, or LPHN2^{-}
447 GPR133^{+}) might result in distinct intracellular cAMP signalling patterns, which may cause
448 differences in membrane excitability or neurotransmitter release from specific spiral ganglion
449 neurons (SGNs). We further hypothesized that the potential involvement of other
450 mechanosensitive GPCRs may increase the temporal and spatial complexity of the information

input.

Our study also reveals that a previously uncharacterized vestibular MET-regulating ion channel CNGA3, in addition to TMC1/2 and proton-conducting Otopetrin-1[36], is essential for equilibrioception. Here, our results suggested that CNGA3 channel activity is coupled with the activation of at least two mechanosensitive GPCRs, GPR133 and LPHN2, and likely in response to changes in intracellular cAMP levels, modulates the membrane excitability of vestibular hair cells during force sensation. Whereas LPHN2 activates the CNGA3 channel and induces membrane depolarization, GPR133 inhibits CNGA3 channel activation and induces membrane hyperpolarization. Importantly, inhibiting CNGA3 activity eliminates LPHN2-mediated MET both *in vitro* and *in vivo*, leading to significant balance dysfunction in mice. Kinetics analysis of LPHN2-CNGA3 coupling revealed that the delayed time between force application and the electrophysiological response was approximately 704.73 ± 8.99 ms, which is close to that recorded for GPR133-CNGA3 coupling (658.0±11.14 ms). Therefore, we speculated that equilibrioception regulated by certain GPCRs in the vestibular system might be a relatively long process, which opposes the traditional views on hearing sensation and equilibrioception[37,38]. Notably, CNG family members play essential roles in vision and olfaction by converting the intracellular chemical signals carried by second messengers to electrical signals[25]. In particular, whereas the rod photoreceptor cells mediating vision in dim light contain CNGA1-CNGB heteromeric channels, the cone photoreceptor cells responsible for bright light perception and colour vision have CNGA3-CNGB3 channels. Moreover, CNG channels in olfactory neurons are composed of CNGA2-CNGA4-CNGB1b subunits. Our results indicated an essential role of CNGA3 in equilibrioception in utricular hair cells and further supported the functional importance of the GPCR-CNG axis in the regulation of basic senses. However, whether CNGA3 forms homomeric channels in vestibular hair cells or interacts with other CNG subunits to form heteromeric channels awaits further investigation. Due to its functional importance in cone photoreceptor cells, CNGA3 mutation is one of the most common causes of achromatopsia, an inherited eye disease associated with congenital absence of cone photoreceptor function[39]. Although the vestibular functions of the affected individuals have rarely been reported, they usually suffer from nystagmus, one of the typical syndromes of vestibular diseases[40]. Therefore, it will be of interest to investigate the pathophysiological

effects of these CNGA3 mutations on the vestibular system, which will provide further insight into CNGA3 functions.

In conclusion, we identified a force-sensitive GPCR expressed in the cuticular plate of vestibular hair cells that is essential for equilibrioception and mediates MET by increasing intracellular cAMP levels and modulating CNGA3 activity. Our results indicated that GPCRs could be direct force sensors during equilibrioception.

Data availability

All data are included in the main text or the extended materials. Data are available when requested from the corresponding authors.

Acknowledgments

This work was supported by National Key R&D Program of China (2019YFA0904200 to J.-P.S., 2021YFA1101300 to R.-J.C.), National Science Fund for Distinguished Young Scholars Grant (81825022 to J.-P.S., 82225011 to X.Y.), National Natural Science Foundation of China (32130055 and 81773704 to J.-P.S., 92057121 to X.Y., 82030029 to R.-J.C., 82271176 to W.-W.L.), the Key Research Project of the Beijing Natural Science Foundation, China (Z200019 to J.-P.S.), Major Fundamental Research Program of Natural Science Foundation of Shandong Province, China (ZR2020ZD39 to J.-P.S. and W.-W.L, ZR2021ZD18 to X.Y.), Taishan Scholars Program of Shandong Province (tsqn201909189 to W.-W.L.).

Author contributions

J.-P.S., X.Y. and R.-J.C initiated, designed and supervised the overall project. J.-P.S., X.Y. and Z.Y. starting the screening of mechanosensitive GPCRs in vestibular and cochlear systems from 2019. R.-J.C provided guidance and suggestions on the vestibular and cochlear studies. Z.Y. and J.-P.S. developed the magnetic force stimulation assay to examine the activation of G proteins and second messengers downstream of GPCRs. X.Y. designed and supervised all electrophysiology experiments. Z.Y., S.-H.Z. and Q.-Y.Z. performed the cell-based assay of LPHNs. S.-H.Z., Z.Y., Q.-Y.Z. and Z.-C.S. performed the electrophysiological experiments and Ca^{2+} imaging supervised by J.-P.S. and X.Y.. J.-P.S., Z.Y., S.-H.Z. and W.-W.L. participated in

511 the design of gene knockout mice and modified AAV-ie. Z.Y., S.-H.Z., Q.-Y.Z. and W.-W.L.
512 performed vestibular behaviour studies. Z.Y., S.-H.Z., Q.-Y.Z. and Y.G. isolated mouse utricle
513 and performed immunofluorescence studies and ex vivo experiments. Z.Y., M.-W.W., S.-H.Z.,
514 and Q.-Y.Z. performed single cell qRT-PCR. Y.G., M.-W.W., S.-H.Z. and Y.-N.S. performed
515 coimmunoprecipitation and western blotting analyses. Z.Y., S.-H.Z., Q.-Y.Z. and W.-W.L.
516 performed the AAV-ie-related experiments under the supervision of J.-P.S. and R.-J.C.. J.-P.S.,
517 X.Y., R.-J.C., Z.Y., S.-H.Z., Q.-Y.Z., Y.S. and W.Y. participated in data analysis and
518 interpretation. Y.S. provided insightful ideas related to the balance sensation based on clinical
519 practice. Z.Y., S.-H.Z., and Q.-Y.Z. prepared the figures. J.-P.S., X.Y., Z.Y. and R.-J.C wrote
520 the manuscript. All the authors have seen and commented on the manuscript.
521
522 **Competing interests**
523 The authors declare no competing interests.
524
525 **Submission history**
526 The manuscript was submitted on Sep 20, 2023 and was sent for peer review on Sep 26, 2023
527 by the journal editor.
528
529 **Figure Legends**
530 **Figure 1. Deficiency of mechanosensitive LPHN2 but not LPHN3 impairs balance in**
531 **mice**
532 **(A)** Schematic representation of the potential roles of TMC1/2 and GPCRs in MET in vestibular
533 hair cells.
534 **(B)** Expression frequency of LPHN subfamily members in mouse utricular hair cells. Data
535 represent the average values of the LPHN expression frequency from a single-cell RNA-seq
536 dataset (GSE71982) and the results of single-hair-cell qRT–PCR analysis in the current study.
537 **(C)** The mRNA levels of LPHN subfamily members in mouse utricular hair cells measured by
538 single-cell qRT–PCR, using their respective expression levels in the brain as a reference
539 (normalized to 1) (n=3). Data are correlated to Figure S1B.
540 **(D-E)** Gi3 (**D**) or Gs (**E**) activation in HEK293 cells overexpressing different LPHNs in

541 response to 3 pN force stimulation measured by G protein dissociation BRET assay (n=3).
542 HEK293 cells transfected with the empty vector pcDNA3.1 and G protein probes were used as
543 a negative control.
544 **(F)** Schematic view (left) and representative tracks (right) of WT, *Lphn2*$^{+/-}$, and *Lphn3*$^{+/-}$ mice
545 in open-field test during 2 min or 10 min tracking period.
546 **(G-I)** Quantification of the circling and travelling activity in open-field test (**G**), duration time
547 on the rotating rod (**H**), and swimming scores (**I**) of WT, *Lphn2*$^{+/-}$, and *Lphn3*$^{+/-}$ mice (n=9 mice
548 per group).
549 **(J)** Schematic view (left) and representative recording curves (right) of the VOR response of
550 WT, *Lphn2*$^{+/-}$, and *Lphn3*$^{+/-}$ mice to earth-vertical axis rotation (0.20-1.5 Hz, 40°/s peak velocity
551 sinusoidal, whole-body passive rotation).
552 **(K)** Quantification of the VOR gain response of WT, *Lphn2*$^{+/-}$, and *Lphn3*$^{+/-}$ mice to earth-
553 vertical axis rotation (n=9 mice per group).
554 **(L)** Schematic view (left) and representative recording curves (right) of the VOR response of
555 WT, *Lphn2*$^{+/-}$, and *Lphn3*$^{+/-}$ mice to off-vertical axis rotation (50°/s, whole-body passive
556 rotation).
557 **(M)** Quantification of the VOR gain response of WT, *Lphn2*$^{+/-}$, and *Lphn3*$^{+/-}$ mice to off-vertical
558 axis rotation (n=9 mice per group).
559 (**D-E**) *P < 0.05; **P < 0.01; ns, no significant difference. HEK293 cells transfected with
560 LPHNs compared with those transfected with pcDNA3.1. (**G-I, K, M**) **P < 0.01; ***P <
561 0.001; ns, no significant difference. Gene knockout mice compared with WT mice. The bars
562 indicate mean ± SEM values. All data were statistically analysed using one-way ANOVA with
563 Dunnett's post hoc test.
564
565 **Figure 2. LPHN2 is specifically expressed at the cuticular plate of utricular hair cells**
566 **(A)** Coimmunostaining of LPHN2 (green) with Myosin7a (red) in utricle whole mounts derived
567 from WT mice at P40 or from *Lphn2*$^{-/-}$ mouse embryos at E18 (n = 3 mice per group). Scale
568 bar, 50 μm.
569 **(B)** Representative images of whole-mount RNAscope in situ hybridization of LPHN2 (white)
570 combined with immunostaining of Myosin7a (red) in the utricle of P40 mice (n = 3 mice).

571 Arrows indicate LPHN2 staining in myosin7a-expressing hair cells. Scale bars, 50 μm and 10
572 μm for low- and high-magnification views, respectively.
573 **(C)** Quantitative analysis of LPHN2 expression in myosin7a-positive utricular hair cells from
574 WT mice or *Lphn2*$^{-/-}$ embryos. Data are correlated to Fig. 2a-b (n = 3 mice per group).
575 **(D)** Left panel: Diagram of utricular hair cells showing the selected optical planes (stereocilia,
576 cuticular plate or basolateral section) for imaging by confocal microscopy. Right panel:
577 Coimmunostaining of spectrin (red), LPHN2 (green) and phalloidin (magenta) at different
578 optical planes of hair cells in utricle whole mounts derived from WT mice (P40) or from *Lphn2*$^{-}$
579 $^{/-}$ embryos (E18). Arrows indicate coimmunostaining of LPHN2 with spectrin at the cuticular
580 plate. The line of polarity reversal (LPR) is depicted as a white dotted line. Scale bar, 10 μm.
581 **(E)** Left panel: Schematic view of LPHN2 (red) expression in utricular hair cells. Right panel:
582 Coimmunostaining of LPHN2 (green) with Myosin7a (red) or SOX2 (magenta) in utricle
583 sections derived from WT mice at P40 (n = 3 mice per group). Arrows indicate the distribution
584 of LPHN2 immunofluorescence puncta at the cuticular plate of utricular hair cells (depicted by
585 white dotted lines). Scale bars, 50 μm and 10 μm for low- and high-magnification views,
586 respectively.
587
588 **Figure 3. Conditional knockout of LPHN2 in mouse hair cells impaired balance**
589 **(A)** Schematic representation of the crossbreeding strategy to generate hair cell-specific *Lphn2*
590 knockout mice and vestibular function analysis.
591 **(B)** Immunostaining of LPHN2 (magenta) and POU4F3 (magenta) in utricle whole mounts
592 derived from *Pou4f3-CreER*$^{+/-}$*Lphn2*$^{fl/fl}$ mice (referred to as *Pc-Lphn2*$^{fl/fl}$) or *Pou4f3-CreER*$^{+/-}$
593 *Lphn2*$^{+/+}$ mice (referred to as *Pc-Lphn2*$^{+/+}$). Enlarged images show the ablation of LPHN2 in
594 the utricular hair cells of *Pc-Lphn2*$^{fl/fl}$ mice (n=3 mice per group). Scale bar: 50 μm and 20 μm
595 for low and high magnification views, respectively.
596 **(C-F)** Quantification of the swimming scores (**C**), time on the rotating rod (**D**), circling activity
597 (**E**) and travelling activity (**F**) in the open field test of *Pc-Lphn2*$^{fl/fl}$ mice and *Pc-Lphn2*$^{+/+}$ mice
598 (n=8 mice per group).
599 **(G)** Representative recording curves (top) and quantification of the VOR gain response (bottom)
600 of *Pc-Lphn2*$^{fl/fl}$ mice and *Pc-Lphn2*$^{+/+}$ mice to earth-vertical axis rotation (n=8 mice per group).

601 **(H)** Representative recording curves (left) and quantification of the VOR gain response (right)
602 of *Pc-Lphn2*$^{fl/fl}$ mice and *Pc-Lphn2*$^{+/+}$ mice to off-vertical axis rotation (n=8 mice per group).
603
604 (**C-H**) *P < 0.05; **P < 0.01; ***P < 0.001; ns, no significant difference. *Pc-Lphn2*$^{fl/fl}$ mice
605 compared with *Pc-Lphn2*$^{+/+}$ mice. The bars indicate mean ± SEM values. All data were
606 statistically analysed using unpaired two-sided Student's *t* test.
607
608
609 **Figure 4. Force sensation by LPHN2 induces Ca^{2+} influx in utricular hair cells by**
610 **activating Gs-cAMP signalling**
611 **(A)** Dose-dependent cAMP production in LPHN2-overexpressing HEK293 cells in response to
612 force applied by LPHN2-M-beads. Polylysine-coated beads (Ctrl-beads) were used as a
613 negative control (n=3).
614 **(B)** cAMP production in utricle explants derived from *Pc-Lphn2*$^{fl/fl}$ mice and *Pc-Lphn2*$^{+/+}$ mice
615 in response to stimulation with 3 pN force or 10 μM forskolin (n=3).
616 **(C)** mRNA levels of different G protein subtypes in the utricle sensory epithelium using their
617 respective expression levels in the brain as a reference (normalized to 1) (n=3).
618 **(D)** Heatmap showing the relative mRNA levels of G protein subtypes in 15 isolated LPHN2-
619 expressing utricular hair cells measured by single-cell qRT–PCR. Data are normalized to the
620 respective expression levels of these G protein subtypes in the brain.
621 **(E-F)** Dose-dependent Gs (**E**) or Gi3 (**F**) activation in LPHN2-overexpressing HEK293 cells
622 in response to force applied by LPHN2-M-beads or Ctrl-beads (n=3).
623 **(G)** Summary of the potency of force-induced Gs or Gi subtype activation in LPHN2-
624 overexpressing HEK293 cells (n=3). Data are correlated to Figure 4E-4F and Figure S4C-S4F.
625 **(H)**Schematic illustration of Ca^{2+} imaging in mouse utricular hair cells labelled with AAV-ie-
626 *Lphn2pr*-mCherry in response to force stimulation.
627 **(I)** Heatmaps showing the Ca^{2+} responses in individual utricular hair cells derived from *Pc-*
628 *Lphn2*$^{+/+}$ mice labelled with AAV-ie-*Lphn2pr*-mCherry (n = 84 cells from 11 mice). The vertical
629 dashed line denotes the onset of force application (0 s). Each row represents the temporal Ca^{2+}
630 response of one hair cell.

(J) Representative Ca^{2+} traces recorded in individual utricular hair cells derived from *Pc-Lphn2*$^{fl/fl}$ or *Pc-Lphn2*$^{+/+}$ mice labelled with AAV-ie-*Lphn2pr*-mCherry.

(K) Proportion of force-sensitive and force-insensitive utricular hair cells derived from *Pc-Lphn2*$^{+/+}$ mice labelled with AAV-ie-*Lphn2pr*-mCherry. Data are correlated to Fig. 4i.

(L) Effect of NF449, PKI 14-22 or YM-254890 treatment on the force-induced Ca^{2+} response in utricular hair cells labelled with AAV-ie-*Lphn2pr*-mCherry (n=10 cells per group).

(M) IP3 levels in the utricle explant of WT mice in response to stimulation with 3 pN force (n=3).

(N) Effect of Ca^{2+} ablation in the incubation buffer on the force-induced Ca^{2+} response in LPHN2-positive utricular hair cells (n=10).

(**B, M**) **P < 0.01; ns, no significant difference. Utricle explants treated with force or forskolin compared with control utricle explants. (**L**) ***P < 0.001; ns, no significant difference. Utricular hair cells treated with inhibitors compared with the control utricular hair cells. (**N**) ***P < 0.001. Utricular hair cells incubated with Ca^{2+}-free buffer compared with the control cells. The bars indicate mean ± SEM values. All data were statistically analysed using one-way ANOVA with Dunnett's post hoc test (**B**) or Student's *t* test (**L-N**).

Fig. 5 | Force-induced LPHN2 activation regulates the membrane excitability of utricular hair cells

(A-B) Representative whole-cell currents (upper panel) elicited by voltage steps between -100 mV and +100 mV and the corresponding I-V curves (lower panel) in AAV-ie-*Lphn2pr*-mCherry-labelled cluster I (**A**) or cluster II (**B**) utricular hair cells derived from *Pc-Lphn2*$^{fl/fl}$ or *Pc-Lphn2*$^{+/+}$ mice in response to force (3 pN) stimulation. n=17 for cluster I cells and n=36 for cluster II cells in *Pc-Lphn2*$^{+/+}$ mice. n=13 for cluster I cells and n=26 for cluster II cells in *Pc-Lphn2*$^{fl/fl}$ mice.

(C) Proportion of force-sensitive and force-insensitive utricular hair cells labelled with AAV-ie-*Lphn2pr*-mCherry derived from *Pc-Lphn2*$^{+/+}$ mice. Data are correlated to Fig. 5a-b.

(D) Representative force-induced membrane potential alteration of cluster I utricular hair cells derived from *Pc-Lphn2*$^{fl/fl}$ or *Pc-Lphn2*$^{+/+}$ mice when holding at absolute zero current (n=10).

661 The time latency between force application or force removal and the change in membrane
662 potential was defined as T_{pr} and T_{po}, respectively. The calculated time constant for the response
663 and the recovery time constant were denoted as τ_p and τ_{rec}, respectively.
664 **(E)** The calculated time parameters in force-stimulated membrane potential alteration of cluster
665 I utricular hair cells (n=10).
666 **(F)** Representative whole-cell currents in cluster I hair cells derived from *Pc-Lphn2*$^{+/+}$ mice in
667 response to 3 pN force stimulation at a holding potential of +100 mV or -70 mV (n=3).
668 **(G)** Effect of NF449 treatment on the whole-cell current in *Pc-Lphn2*$^{+/+}$ cluster I hair cells in
669 response to 3 pN force stimulation (n=11).
670 **(H)** Effect of NF449 treatment on the force-stimulated membrane potential alteration in *Pc-*
671 *Lphn2*$^{+/+}$ cluster I hair cells (n=13).
672
673
674 **Figure 6. LPHN2 regulates MET in utricular hair cells through coupling to CNGA3**
675 **(A)** Expression profiles of cyclic nucleotide–activated ion channels in LPHN2-expressing
676 utricular hair cells. A single-cell RNA-seq dataset (GSE71982) was used in this experiment.
677 **(B)** mRNA levels of CNG and HCN channels in WT cluster I and cluster II utricular hair cells
678 examined by single-cell qRT–PCR (n=10 cells per cluster). Data are normalized to the
679 respective expression levels of these ion channels in the brain.
680 **(C)** Coimmunoprecipitation of LPHN2 with CNG or HCN channels in mouse utricle cell
681 lysates. Representative blots from three independent experiments are shown (n=3).
682 **(D)** Left panel: Coimmunostaining of LPHN2 (green) with CNGA3 (red) in utricle sections
683 derived from WT mice (n = 3). Scale bar: 10 μm. Right panel: Pearson's correlation analysis of
684 LPHN2 and CNGA3 fluorescence intensities. The Pearson's correlation coefficient was 0.68.
685 **(E)** Representative whole-cell currents (upper panel) elicited by voltage steps between -100 mV
686 and +100 mV and the corresponding I-V curves (lower panel) in HEK293 cells overexpressing
687 LPHN2/CNGA3/CNGB1 (referred to as LPHN2^{+}) or CNGA3/CNGB1 (referred to as LPHN2^{-})
688 in response to force (3 pN) stimulation (n=5).
689 **(F)** Representative whole-cell currents (left) and the corresponding dose–response curves (right)
690 in LPHN2^{+} or LPHN2^{-} HEK293 cells in response to force stimulation at a holding potential of

691 +100 mV (n=3). Data are correlated to Figure S4F.

692 **(G)** Summary of the potency of force-induced cAMP production or membrane potential/current

693 alteration in utricle explants from WT mice or in LPHN2-overexpressing HEK293 cells.

694

695 **Figure 7. Heterozygous hair cell-specific *Cnga3* knockout mice showed impaired balance**

696 **(A)**Representative tracks of *Pc-Cnga3*$^{+/+}$ and *Pc-Cnga3*$^{fl/+}$ mice in the open-field test during a

697 2 min or 10 min tracking period.

698 **(B-E)** Quantification of the circling activity (**B**) and travelling activity (**C**) in the open field test,

699 swimming scores (**D**) and duration time on the rotating rod (**E**) of *Pc-Cnga3*$^{+/+}$ and *Pc-Cnga3*$^{fl/+}$

700 mice (n=10 for *Pc-Cnga3*$^{+/+}$mice and n=6 for *Pc-Cnga3*$^{fl/+}$ mice).

701 **(F)** Representative recording curves (top) and quantification of the VOR gain response (bottom)

702 of *Pc-Cnga3*$^{+/+}$ and *Pc-Cnga3*$^{fl/+}$ mice to earth-vertical axis rotation (n=10 for *Pc-*

703 *Cnga3*$^{+/+}$mice and n=6 for *Pc-Cnga3*$^{fl/+}$ mice).

704 **(G)** Representative recording curves (left) and quantification of the VOR gain response (right)

705 of *Pc-Cnga3*$^{+/+}$ and *Pc-Cnga3*$^{fl/+}$ mice to off-vertical axis rotation (n=10 for *Pc-Cnga3*$^{+/+}$mice

706 and n=6 for *Pc-Cnga3*$^{fl/+}$ mice).

707 **(H)** Representative whole-cell currents (upper) elicited by voltage steps between -100 mV and

708 +100 mV and the corresponding I-V curves (lower) in AAV-ie-*Lphn2pr*-mCherry-labelled

709 cluster I utricular hair cells in response to force (3 pN) stimulation in the absence or presence

710 of 100 μM L-cis-diltiazem (n=10).

711 **(I)** Representative Ca^{2+} traces recorded in individual AAV-ie-*Lphn2pr*-mCherry-labelled

712 utricular hair cells in response to force (3 pN) stimulation in the absence or presence of 100 μM

713 L-cis-diltiazem.

714 **(J)** Quantification of the effect of L-cis-diltiazem treatment on the force-induced Ca^{2+} response

715 in utricular hair cells labelled with AAV-ie-*Lphn2pr*-mCherry (n=10 cells).

716

717 (**B-G**) ***P < 0.001, **P < 0.01; ns, no significant difference. *Pc-Cnga3*$^{fl/+}$ mice compared with

718 *Pc-Cnga3*$^{+/+}$ mice. (**J**) ***P < 0.001. Utricular hair cells treated with L-cis-diltiazem compared

719 with control cells. The bars indicate mean ± SEM values. All data were statistically analysed

720 using unpaired (**B-G**) or paired (**J**) two-sided Student's *t* test.

Figure 8. Specific re-expression of LPHN2 in hair cells rescued the vestibular function of LPHN2-deficient mice

(A-D) Quantification of the circling (**A**) and travelling activity (**B**) in the open-field test during 10 min, swimming scores (**C**) and duration time on the rotating rod (**D**) of *Pc-Lphn2*$^{+/+}$, *Pc-Lphn2*$^{fl/fl}$, AAV-ie-LPHN2 mice and AAV-ie-*Lphn2pr* mice (n=6 mice per group).

(E-F) Representative recording curves (left) and quantification of the VOR gain responses (right) of *Pc-Lphn2*$^{+/+}$, *Pc-Lphn2*$^{fl/fl}$, AAV-ie-LPHN2 mice and AAV-ie-*Lphn2pr* mice to earth-vertical axis (**E**) or off-vertical axis (**F**) rotation (n=6 mice per group).

(G) Representative whole-cell currents (left) elicited by voltage steps between -100 mV and +100 mV and the corresponding I-V curves (right) in cluster I utricular hair cells derived from *Pc-Lphn2*$^{+/+}$, AAV-ie-LPHN2 mice and AAV-ie-*Lphn2pr* mice in response to force (3 pN) stimulation (n=5, 7, and 6 for *Pc-Lphn2*$^{+/+}$, AAV-ie-LPHN2 and AAV-ie-*Lphn2pr* group, respectively).

(**A-F**) *P < 0.05; **P < 0.01; ***P < 0.001; ns, no significant difference. *Pc-Lphn2*$^{fl/fl}$ mice compared with *Pc-Lphn2*$^{+/+}$ mice. The bars indicate mean ± SEM values. All data were statistically analysed using one-way ANOVA with Dunnett's post hoc test.

References

1 Cullen, K. E. Vestibular processing during natural self-motion: implications for perception and action. *Nat Rev Neurosci* **20**, 346-363, doi:10.1038/s41583-019-0153-1 (2019).

2 Eatock, R. A. & Songer, J. E. Vestibular hair cells and afferents: two channels for head motion signals. *Annu Rev Neurosci* **34**, 501-534, doi:10.1146/annurev-neuro-061010-113710 (2011).

3 Zheng, W. & Holt, J. R. The Mechanosensory Transduction Machinery in Inner Ear Hair Cells. *Annu Rev Biophys* **50**, 31-51, doi:10.1146/annurev-biophys-062420-081842 (2021).

751 4 Cunningham, C. L. & Muller, U. Molecular Structure of the Hair Cell
752 Mechanoelectrical Transduction Complex. *Cold Spring Harb Perspect Med* **9**,
753 doi:10.1101/cshperspect.a033167 (2019).
754 5 Kindt, K. S. *et al.* EMX2-GPR156-Galphai reverses hair cell orientation in
755 mechanosensory epithelia. *Nat Commun* **12**, 2861, doi:10.1038/s41467-021-22997-1
756 (2021).
757 6 Zhang, Z. & Chai, R. Hear the sounds: the role of G protein-coupled receptors in the
758 cochlea. *Am J Physiol Cell Physiol* **323**, C1088-C1099,
759 doi:10.1152/ajpcell.00453.2021 (2022).
760 7 Duncan, J. S. *et al.* Celsr1 coordinates the planar polarity of vestibular hair cells during
761 inner ear development. *Dev Biol* **423**, 126-137, doi:10.1016/j.ydbio.2017.01.020
762 (2017).
763 8 Yau, K. W. & Hardie, R. C. Phototransduction motifs and variations. *Cell* **139**, 246-264,
764 doi:10.1016/j.cell.2009.09.029 (2009).
765 9 Chen, T. Y. & Yau, K. W. Direct modulation by Ca(2+)-calmodulin of cyclic nucleotide-
766 activated channel of rat olfactory receptor neurons. *Nature* **368**, 545-548,
767 doi:10.1038/368545a0 (1994).
768 10 Chandrashekar, J., Hoon, M. A., Ryba, N. J. & Zuker, C. S. The receptors and cells for
769 mammalian taste. *Nature* **444**, 288-294, doi:10.1038/nature05401 (2006).
770 11 Burns, J. C., Kelly, M. C., Hoa, M., Morell, R. J. & Kelley, M. W. Single-cell RNA-
771 Seq resolves cellular complexity in sensory organs from the neonatal inner ear. *Nat*
772 *Commun* **6**, 8557, doi:10.1038/ncomms9557 (2015).
773 12 Anderson, G. R. *et al.* Postsynaptic adhesion GPCR latrophilin-2 mediates target
774 recognition in entorhinal-hippocampal synapse assembly. *J Cell Biol* **216**, 3831-3846,
775 doi:10.1083/jcb.201703042 (2017).
776 13 Sando, R., Jiang, X. & Sudhof, T. C. Latrophilin GPCRs direct synapse specificity by
777 coincident binding of FLRTs and teneurins. *Science* **363**, doi:10.1126/science.aav7969
778 (2019).
779 14 Liu, Y. *et al.* Critical role of spectrin in hearing development and deafness. *Sci Adv* **5**,
780 eaav7803, doi:10.1126/sciadv.aav7803 (2019).

15 Cortese, M. *et al.* Spectrin betaV adaptive mutations and changes in subcellular location correlate with emergence of hair cell electromotility in mammalians. *Proc Natl Acad Sci U S A* **114**, 2054-2059, doi:10.1073/pnas.1618778114 (2017).

16 Vahava, O. *et al.* Mutation in transcription factor POU4F3 associated with inherited progressive hearing loss in humans. *Science* **279**, 1950-1954, doi:10.1126/science.279.5358.1950 (1998).

17 Nakamura, T. & Gold, G. H. A cyclic nucleotide-gated conductance in olfactory receptor cilia. *Nature* **325**, 442-444, doi:10.1038/325442a0 (1987).

18 Zhang, Y. *et al.* Coding of sweet, bitter, and umami tastes: different receptor cells sharing similar signaling pathways. *Cell* **112**, 293-301, doi:10.1016/s0092-8674(03)00071-0 (2003).

19 Arshavsky, V. & Bownds, M. D. Regulation of deactivation of photoreceptor G protein by its target enzyme and cGMP. *Nature* **357**, 416-417, doi:10.1038/357416a0 (1992).

20 Nakatani, K. & Yau, K. W. Calcium and light adaptation in retinal rods and cones. *Nature* **334**, 69-71, doi:10.1038/334069a0 (1988).

21 Taruno, A. *et al.* CALHM1 ion channel mediates purinergic neurotransmission of sweet, bitter and umami tastes. *Nature* **495**, 223-226, doi:10.1038/nature11906 (2013).

22 Street, V. A., McKee-Johnson, J. W., Fonseca, R. C., Tempel, B. L. & Noben-Trauth, K. Mutations in a plasma membrane Ca2+-ATPase gene cause deafness in deafwaddler mice. *Nat Genet* **19**, 390-394, doi:10.1038/1284 (1998).

23 Beutner, D., Voets, T., Neher, E. & Moser, T. Calcium dependence of exocytosis and endocytosis at the cochlear inner hair cell afferent synapse. *Neuron* **29**, 681-690, doi:10.1016/s0896-6273(01)00243-4 (2001).

24 Parsons, T. D., Lenzi, D., Almers, W. & Roberts, W. M. Calcium-triggered exocytosis and endocytosis in an isolated presynaptic cell: capacitance measurements in saccular hair cells. *Neuron* **13**, 875-883, doi:10.1016/0896-6273(94)90253-4 (1994).

25 Craven, K. B. & Zagotta, W. N. CNG and HCN channels: two peas, one pod. *Annu Rev Physiol* **68**, 375-401, doi:10.1146/annurev.physiol.68.040104.134728 (2006).

26 Jiang, Z., Yue, W. W. S., Chen, L., Sheng, Y. & Yau, K. W. Cyclic-Nucleotide- and HCN-Channel-Mediated Phototransduction in Intrinsically Photosensitive Retinal

811 Ganglion Cells. *Cell* **175**, 652-664 e612, doi:10.1016/j.cell.2018.08.055 (2018).
812 27 Ping, Y. Q. *et al.* Structural basis for the tethered peptide activation of adhesion GPCRs.
813 *Nature* **604**, 763-770, doi:10.1038/s41586-022-04619-y (2022).
814 28 Xiao, P. *et al.* Tethered peptide activation mechanism of the adhesion GPCRs ADGRG2
815 and ADGRG4. *Nature* **604**, 771-778, doi:10.1038/s41586-022-04590-8 (2022).
816 29 Jia, Y. *et al.* TMC1 and TMC2 Proteins Are Pore-Forming Subunits of
817 Mechanosensitive Ion Channels. *Neuron* **105**, 310-321 e313,
818 doi:10.1016/j.neuron.2019.10.017 (2020).
819 30 Pan, B. *et al.* TMC1 Forms the Pore of Mechanosensory Transduction Channels in
820 Vertebrate Inner Ear Hair Cells. *Neuron* **99**, 736-753 e736,
821 doi:10.1016/j.neuron.2018.07.033 (2018).
822 31 Pan, B. *et al.* TMC1 and TMC2 are components of the mechanotransduction channel
823 in hair cells of the mammalian inner ear. *Neuron* **79**, 504-515,
824 doi:10.1016/j.neuron.2013.06.019 (2013).
825 32 Buck, L. & Axel, R. A novel multigene family may encode odorant receptors: a
826 molecular basis for odor recognition. *Cell* **65**, 175-187, doi:10.1016/0092-
827 8674(91)90418-x (1991).
828 33 Yang, F. *et al.* Structure, function and pharmacology of human itch receptor complexes.
829 *Nature* **600**, 164-169, doi:10.1038/s41586-021-04077-y (2021).
830 34 Wu, Z. *et al.* Mechanosensory hair cells express two molecularly distinct
831 mechanotransduction channels. *Nat Neurosci* **20**, 24-33, doi:10.1038/nn.4449 (2017).
832 35 Firestein, S., Darrow, B. & Shepherd, G. M. Activation of the sensory current in
833 salamander olfactory receptor neurons depends on a G protein-mediated cAMP second
834 messenger system. *Neuron* **6**, 825-835, doi:10.1016/0896-6273(91)90178-3 (1991).
835 36 Hurle, B. *et al.* Non-syndromic vestibular disorder with otoconial agenesis in
836 tilted/mergulhador mice caused by mutations in otopetrin 1. *Hum Mol Genet* **12**, 777-
837 789, doi:10.1093/hmg/ddg087 (2003).
838 37 Fettiplace, R., Ricci, A. J. & Hackney, C. M. Clues to the cochlear amplifier from the
839 turtle ear. *Trends Neurosci* **24**, 169-175, doi:10.1016/s0166-2236(00)01740-9 (2001).
840 38 Fettiplace, R. & Kim, K. X. The physiology of mechanoelectrical transduction channels

in hearing. *Physiol Rev* **94**, 951-986, doi:10.1152/physrev.00038.2013 (2014).

39 Michalakis, S., Becirovic, E. & Biel, M. Retinal Cyclic Nucleotide-Gated Channels: From Pathophysiology to Therapy. *Int J Mol Sci* **19**, doi:10.3390/ijms19030749 (2018).

40 Remmer, M. H., Rastogi, N., Ranka, M. P. & Ceisler, E. J. Achromatopsia: a review. *Curr Opin Ophthalmol* **26**, 333-340, doi:10.1097/ICU.0000000000000189 (2015).

41 Tan, F. *et al.* AAV-ie enables safe and efficient gene transfer to inner ear cells. *Nat Commun* **10**, 3733, doi:10.1038/s41467-019-11687-8 (2019).

Figure 1

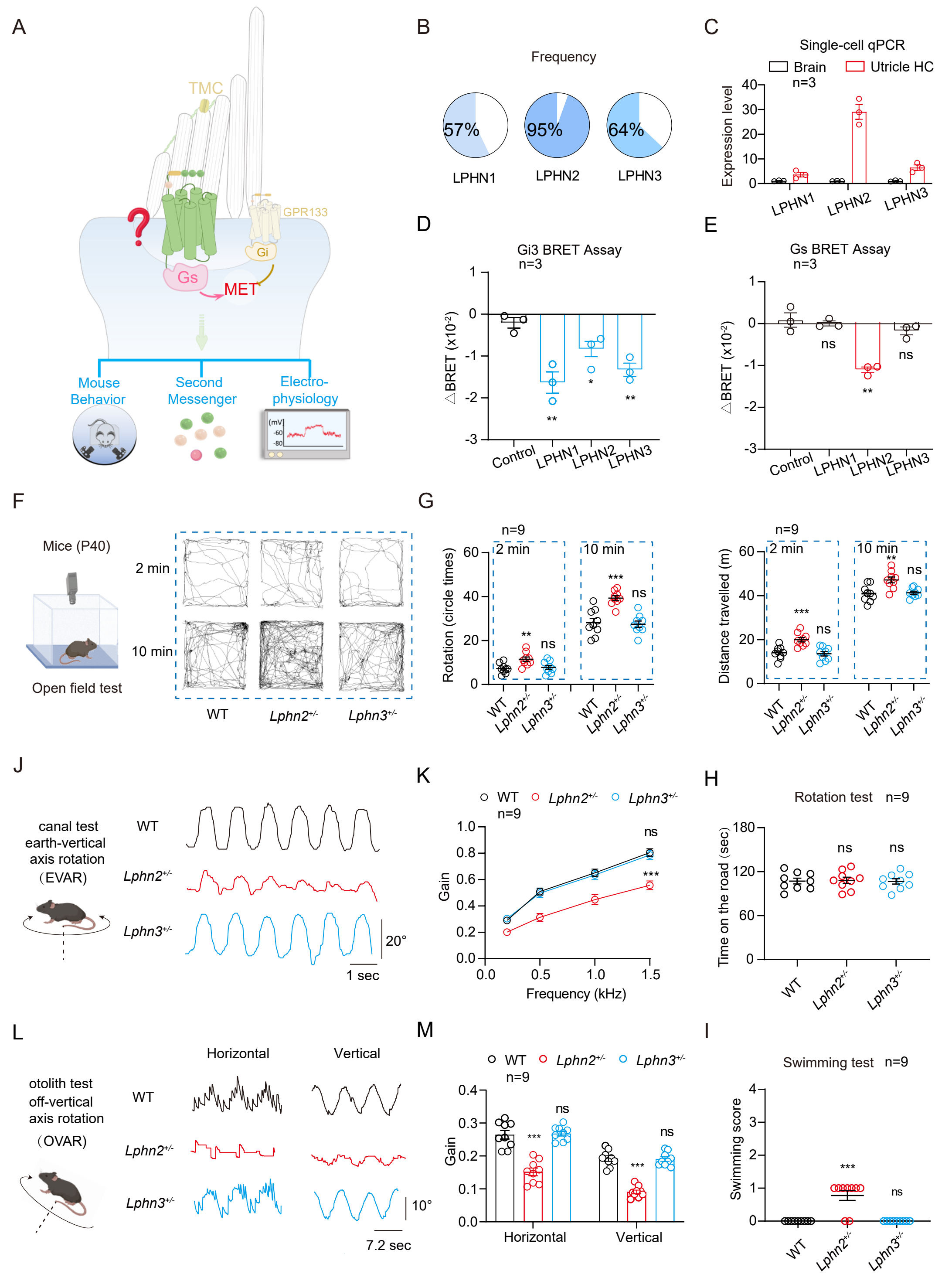
A
TMC
GPR133
Gi
Gs
MET
Mouse Behavior
Second Messenger
Electro-physiology
B
Frequency
57%
95%
64%
LPHN1
LPHN2
LPHN3
C
Single-cell qPCR
Brain
Utricle HC
n=3
Expression level
LPHN1
LPHN2
LPHN3
D
Gi3 BRET Assay
n=3
△BRET (x10-2)
Control
LPHN1
LPHN2
LPHN3
E
Gs BRET Assay
n=3
△BRET (x10-2)
ns
Control
LPHN1
LPHN2
LPHN3
F
Mice (P40)
Open field test
2 min
10 min
WT
Lphn2+/-
Lphn3+/-
G
n=9
2 min
10 min
Rotation (circle times)
Distance travelled (m)
WT
Lphn2+/-
Lphn3+/-
J
canal test
earth-vertical
axis rotation
(EVAR)
WT
Lphn2+/-
Lphn3+/-
20°
1 sec
K
WT
Lphn2+/-
Lphn3+/-
n=9
Gain
Frequency (kHz)
H
Rotation test n=9
Time on the road (sec)
ns
WT
Lphn2+/-
Lphn3+/-
L
otolith test
off-vertical
axis rotation
(OVAR)
Horizontal
Vertical
WT
Lphn2+/-
Lphn3+/-
10°
7.2 sec
M
WT
Lphn2+/-
Lphn3+/-
n=9
Gain
Horizontal
Vertical
I
Swimming test n=9
Swimming score
WT
Lphn2+/-
Lphn3+/-

Figure 2

A

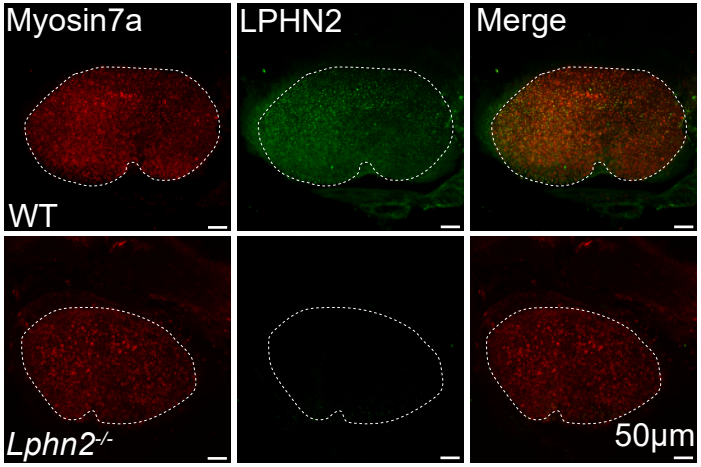

B

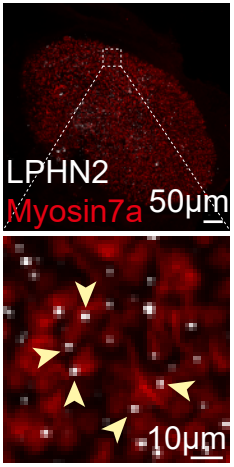

C

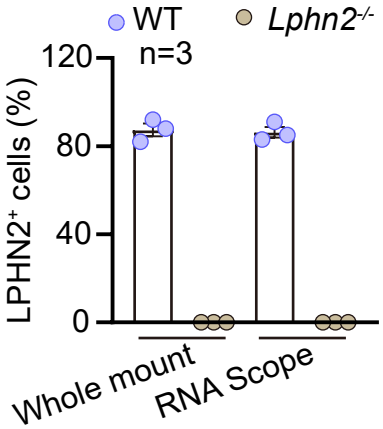

D

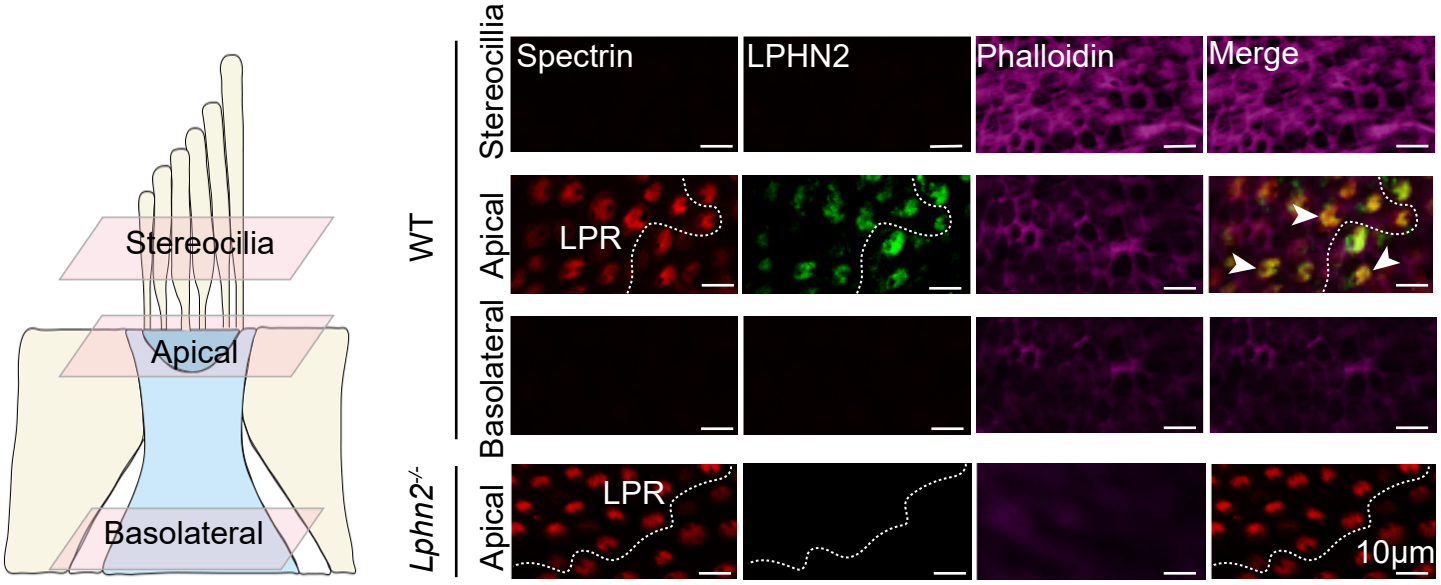

E

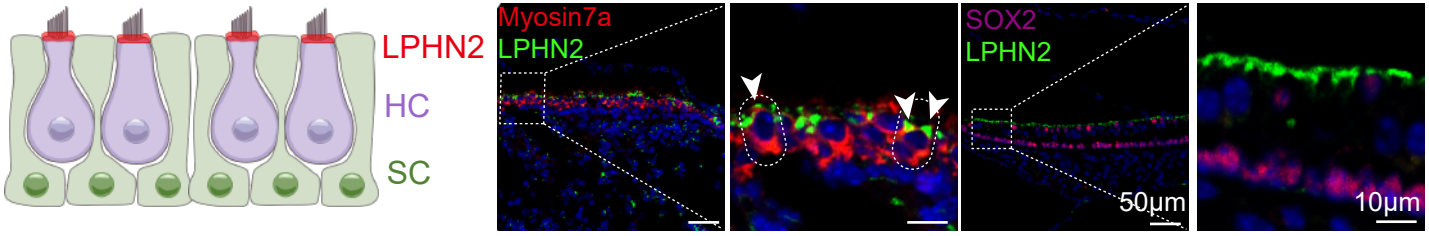

Figure 3

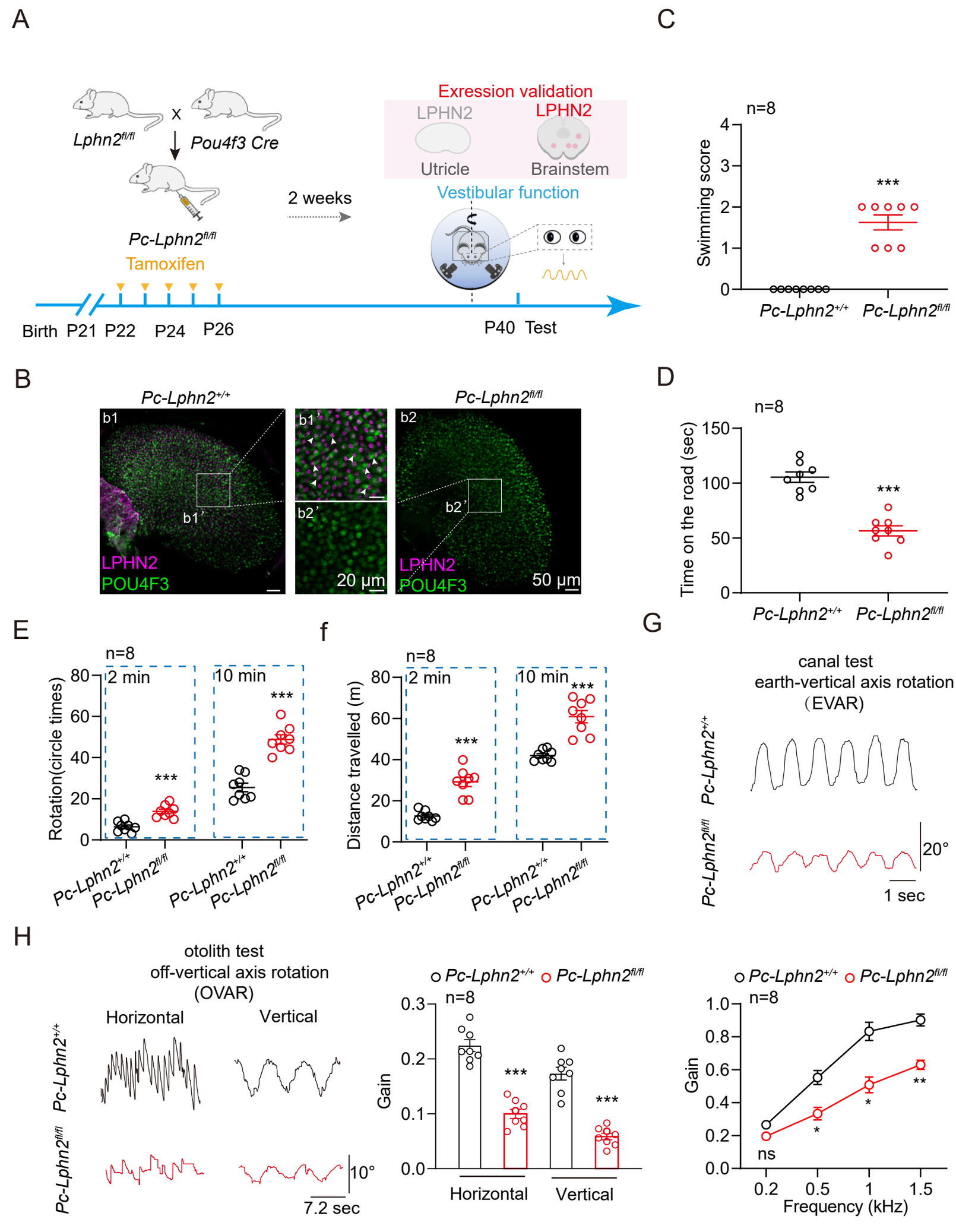
A
Lphn2fl/fl
x
Pou4f3 Cre
Pc-Lphn2fl/fl
Tamoxifen
2 weeks
Exression validation
LPHN2
LPHN2
Utricle
Brainstem
Vestibular function
Birth P21 P22 P24 P26
P40 Test
C
n=8
Swimming score
***
Pc-Lphn2+/+
Pc-Lphn2fl/fl
B
Pc-Lphn2+/+
Pc-Lphn2fl/fl
b1
b1'
b2
b2'
LPHN2
POU4F3
20 μm
50 μm
D
n=8
Time on the road (sec)
***
Pc-Lphn2+/+
Pc-Lphn2fl/fl
E
n=8
Rotation(circle times)
2 min
10 min
***
Pc-Lphn2+/+
Pc-Lphn2fl/fl
f
n=8
Distance travelled (m)
2 min
10 min
***
G
canal test
earth-vertical axis rotation
(EVAR)
Pc-Lphn2+/+
Pc-Lphn2fl/fl
20°
1 sec
H
otolith test
off-vertical axis rotation
(OVAR)
Horizontal
Vertical
10°
7.2 sec
Pc-Lphn2+/+
Pc-Lphn2fl/fl
n=8
Gain
***
Horizontal
Vertical
Pc-Lphn2+/+
Pc-Lphn2fl/fl
n=8
Gain
ns
*
**
Frequency (kHz)

Figure 4

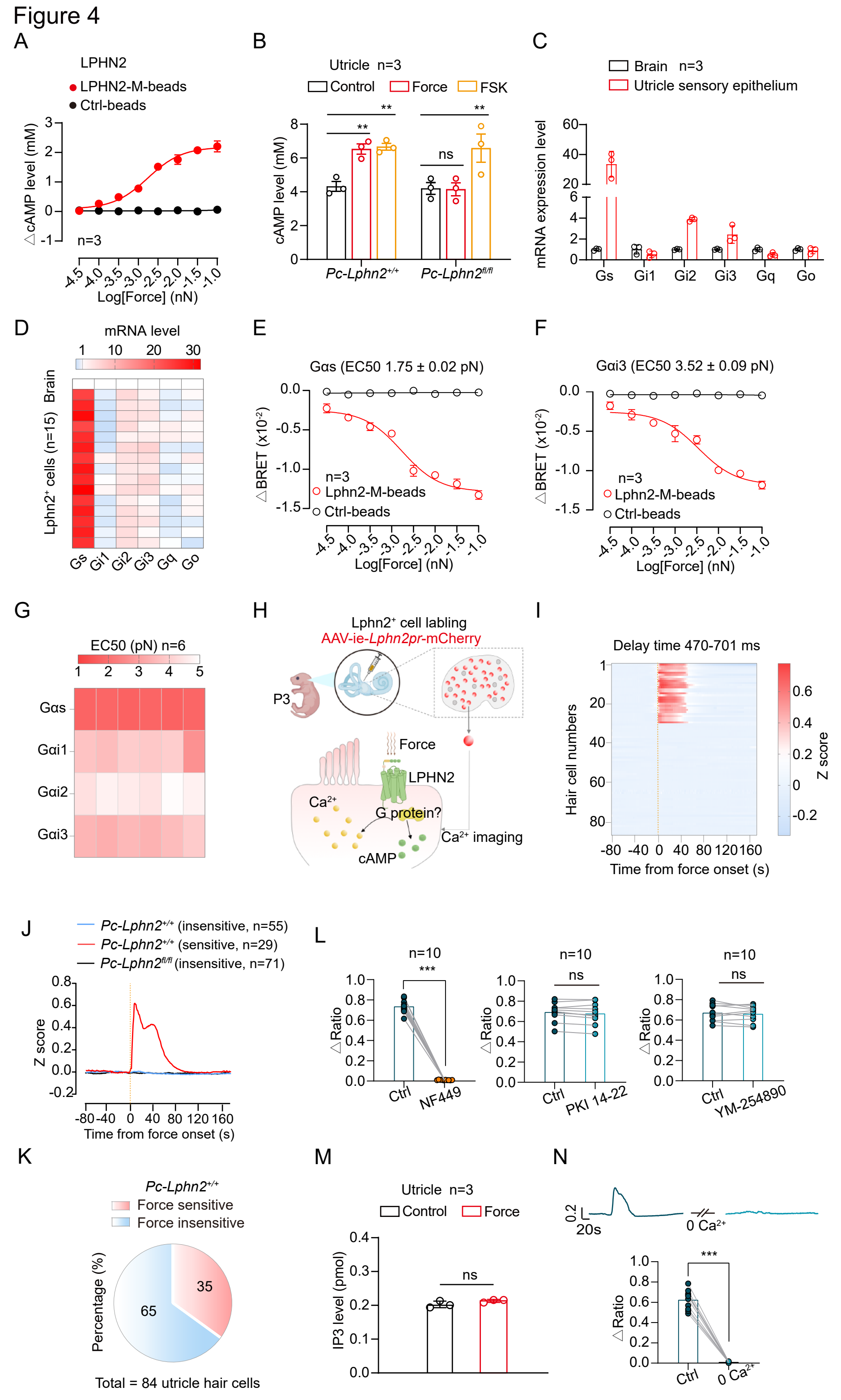
A
LPHN2
LPHN2-M-beads
Ctrl-beads
△cAMP level (mM)
n=3
Log[Force] (nN)
B
Utricle n=3
Control
Force
FSK
cAMP level (mM)
ns
Pc-Lphn2+/+
Pc-Lphn2fl/fl
C
Brain n=3
Utricle sensory epithelium
mRNA expression level
Gs
Gi1
Gi2
Gi3
Gq
Go
D
mRNA level
Lphn2+ cells (n=15)
Brain
E
Gαs (EC50 1.75 ± 0.02 pN)
△BRET (x10-2)
n=3
Lphn2-M-beads
Ctrl-beads
Log[Force] (nN)
F
Gαi3 (EC50 3.52 ± 0.09 pN)
G
EC50 (pN) n=6
Gαs
Gαi1
Gαi2
Gαi3
H
Lphn2+ cell labling
AAV-ie-Lphn2pr-mCherry
P3
Force
LPHN2
Ca2+
G protein?
Ca2+ imaging
cAMP
I
Delay time 470-701 ms
Hair cell numbers
Z score
Time from force onset (s)
J
Pc-Lphn2+/+ (insensitive, n=55)
Pc-Lphn2+/+ (sensitive, n=29)
Pc-Lphn2fl/fl (insensitive, n=71)
Z score
Time from force onset (s)
L
n=10
Ctrl
NF449
PKI 14-22
YM-254890
△Ratio
K
Pc-Lphn2+/+
Force sensitive
Force insensitive
Percentage (%)
35
65
Total = 84 utricle hair cells
M
Utricle n=3
Control
Force
IP3 level (pmol)
ns
N
20s
0 Ca2+
△Ratio

Figure 5

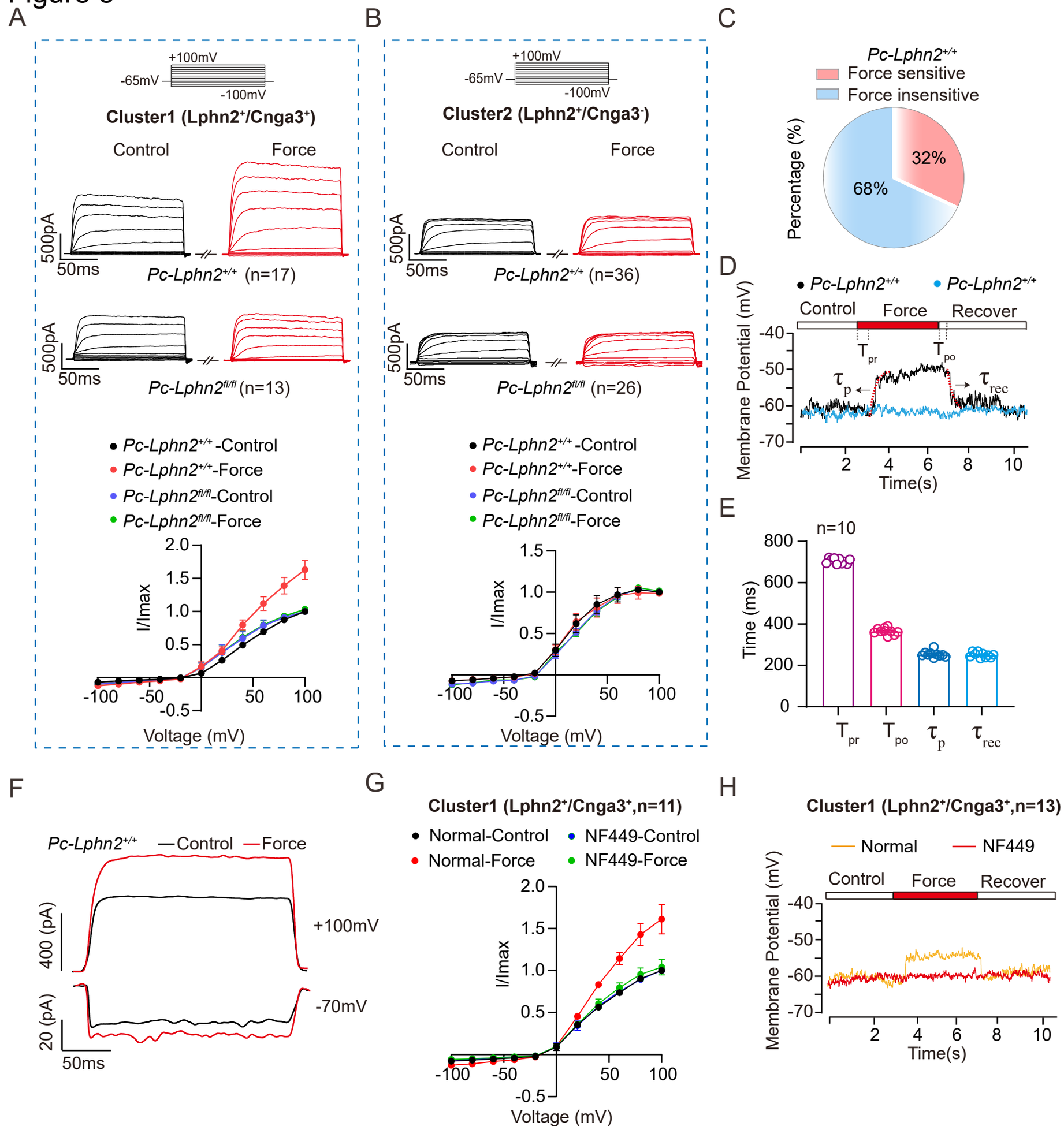
A
+100mV
-65mV
-100mV
Cluster1 (Lphn2+/Cnga3+)
Control
Force
500pA
50ms
Pc-Lphn2+/+ (n=17)
Pc-Lphn2fl/fl (n=13)
Pc-Lphn2+/+-Control
Pc-Lphn2+/+-Force
Pc-Lphn2fl/fl-Control
Pc-Lphn2fl/fl-Force
I/Imax
Voltage (mV)
B
Cluster2 (Lphn2+/Cnga3-)
Pc-Lphn2+/+ (n=36)
Pc-Lphn2fl/fl (n=26)
C
Pc-Lphn2+/+
Force sensitive
Force insensitive
Percentage (%)
32%
68%
D
Pc-Lphn2+/+
Pc-Lphn2+/+
Control
Force
Recover
Membrane Potential (mV)
Tpr
Tpo
τp
τrec
Time(s)
E
n=10
Time (ms)
Tpr
Tpo
τp
τrec
F
Pc-Lphn2+/+
Control
Force
400 (pA)
20 (pA)
+100mV
-70mV
50ms
G
Cluster1 (Lphn2+/Cnga3+,n=11)
Normal-Control
NF449-Control
Normal-Force
NF449-Force
I/Imax
Voltage (mV)
H
Cluster1 (Lphn2+/Cnga3+,n=13)
Normal
NF449
Control
Force
Recover
Membrane Potential (mV)
Time(s)

Figure 6

A

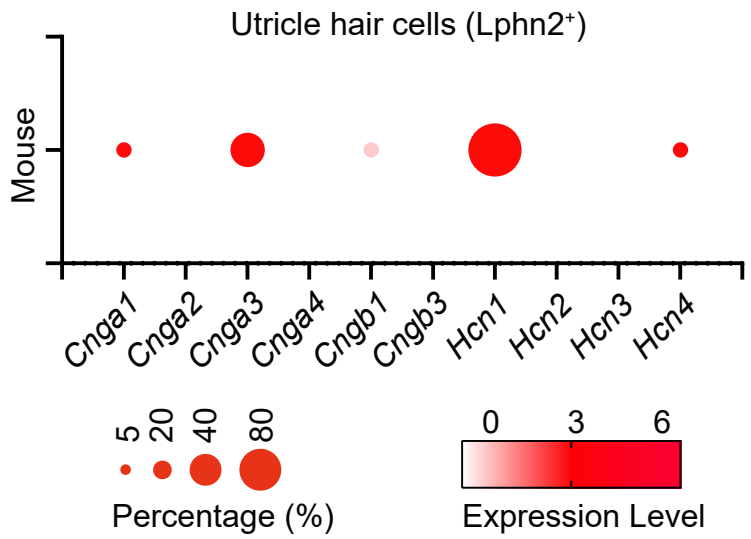

B

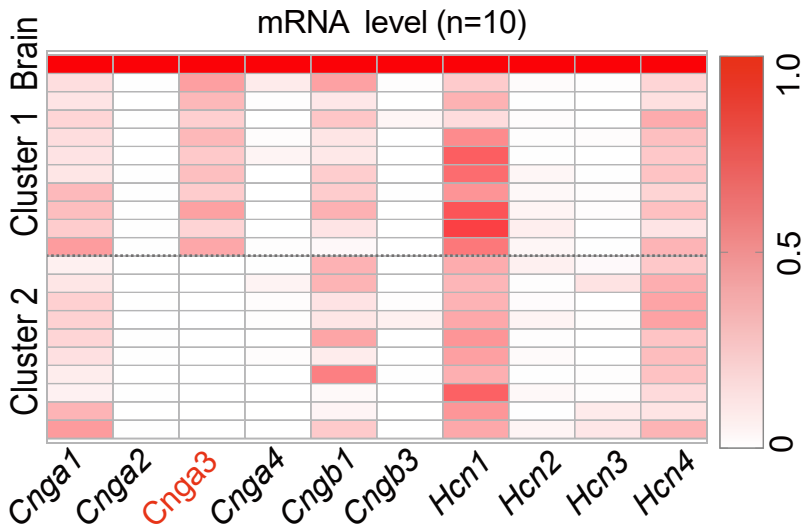

C

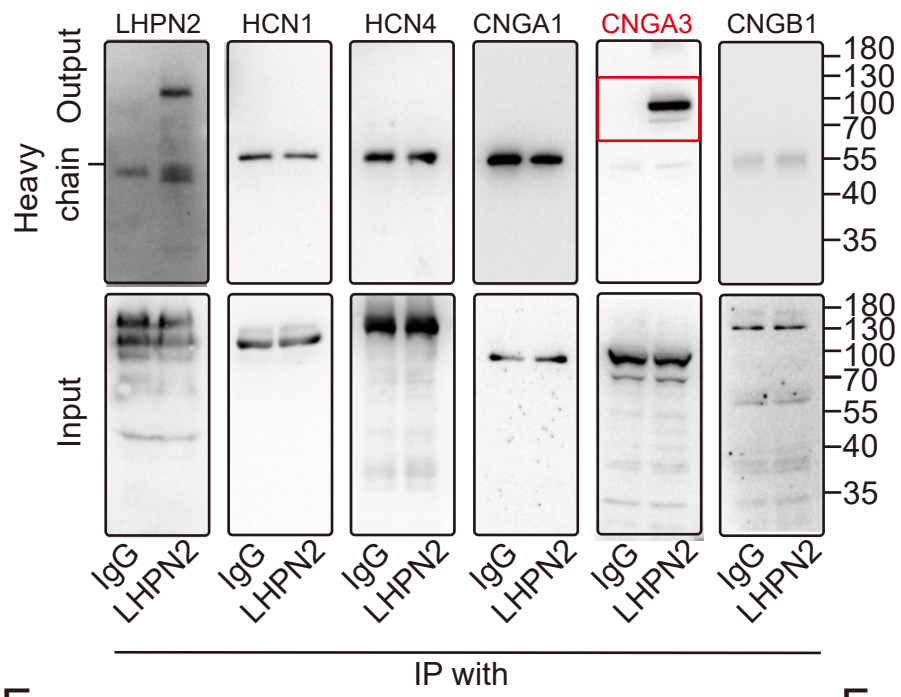

D

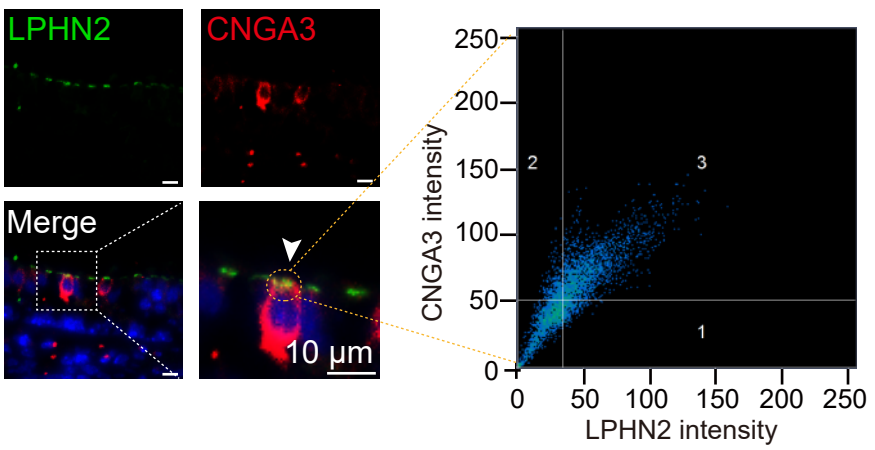

E

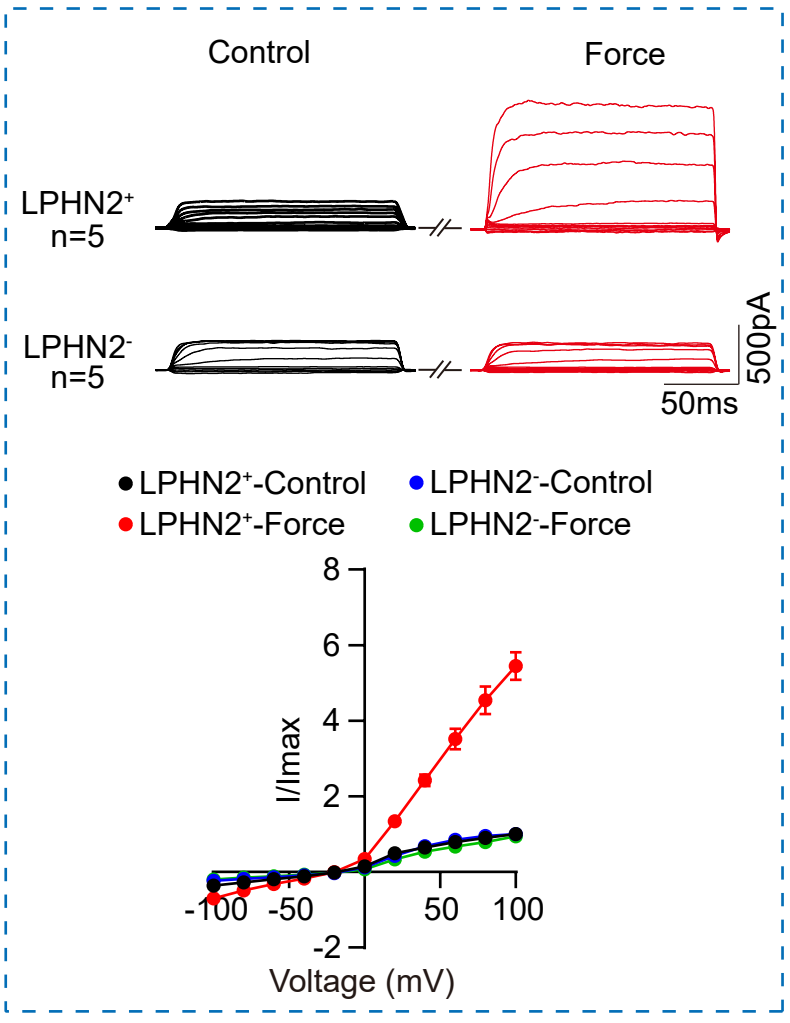

F

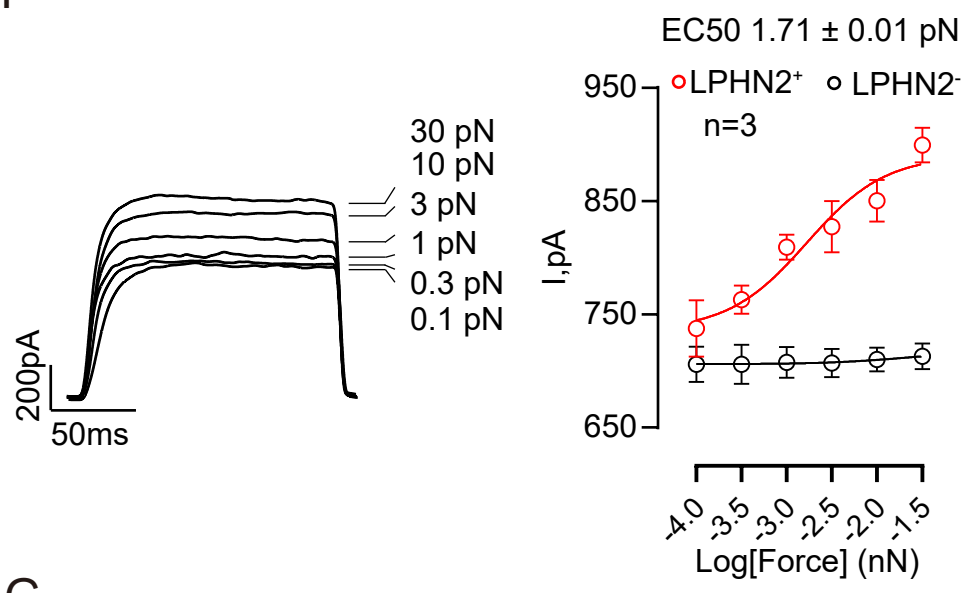

G

LPHN2		EC_{50} (pN)
cAMP level	HEK 293	1.70 ± 0.34
	Utricle	1.64 ± 0.13
potential / current level	HEK 293	1.71 ± 0.01
	Utricle	1.83 ± 0.05

Figure 7

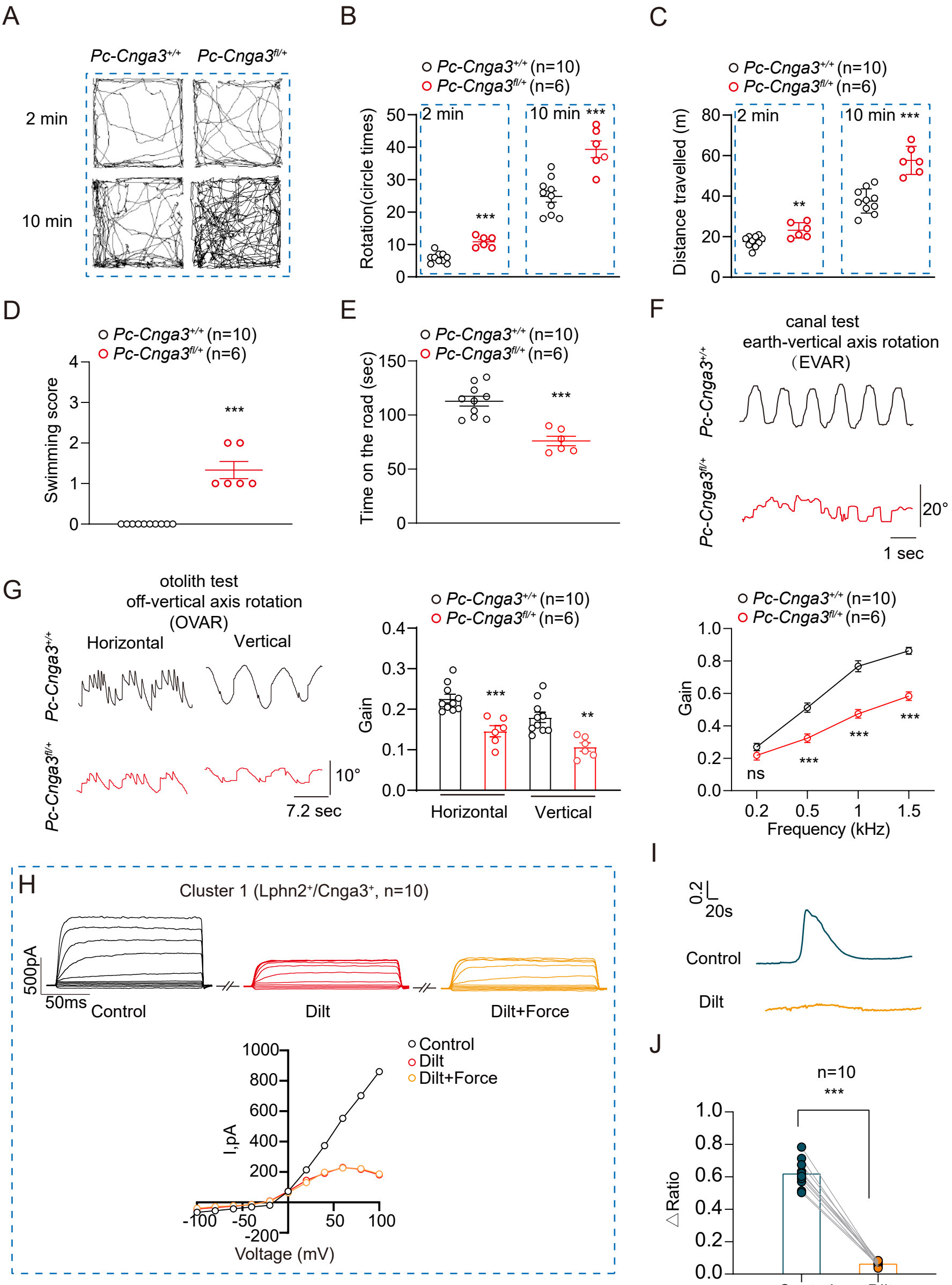
A
Pc-Cnga3+/+
Pc-Cnga3fl/+
2 min
10 min
B
Pc-Cnga3+/+ (n=10)
Pc-Cnga3fl/+ (n=6)
Rotation(circle times)
2 min
10 min
***
C
Pc-Cnga3+/+ (n=10)
Pc-Cnga3fl/+ (n=6)
Distance travelled (m)
2 min
10 min
**
***
D
Pc-Cnga3+/+ (n=10)
Pc-Cnga3fl/+ (n=6)
Swimming score
***
E
Pc-Cnga3+/+ (n=10)
Pc-Cnga3fl/+ (n=6)
Time on the road (sec)
***
F
canal test
earth-vertical axis rotation
(EVAR)
Pc-Cnga3+/+
Pc-Cnga3fl/+
20°
1 sec
G
otolith test
off-vertical axis rotation
(OVAR)
Horizontal
Vertical
Pc-Cnga3+/+
Pc-Cnga3fl/+
10°
7.2 sec
Pc-Cnga3+/+ (n=10)
Pc-Cnga3fl/+ (n=6)
Gain
***
**
Horizontal
Vertical
Pc-Cnga3+/+ (n=10)
Pc-Cnga3fl/+ (n=6)
Gain
ns
***
***
***
Frequency (kHz)
H
Cluster 1 (Lphn2+/Cnga3+, n=10)
500pA
50ms
Control
Dilt
Dilt+Force
Control
Dilt
Dilt+Force
I,pA
Voltage (mV)
I
0.2
20s
Control
Dilt
J
n=10
***
△Ratio
Control
Dilt

Figure 8

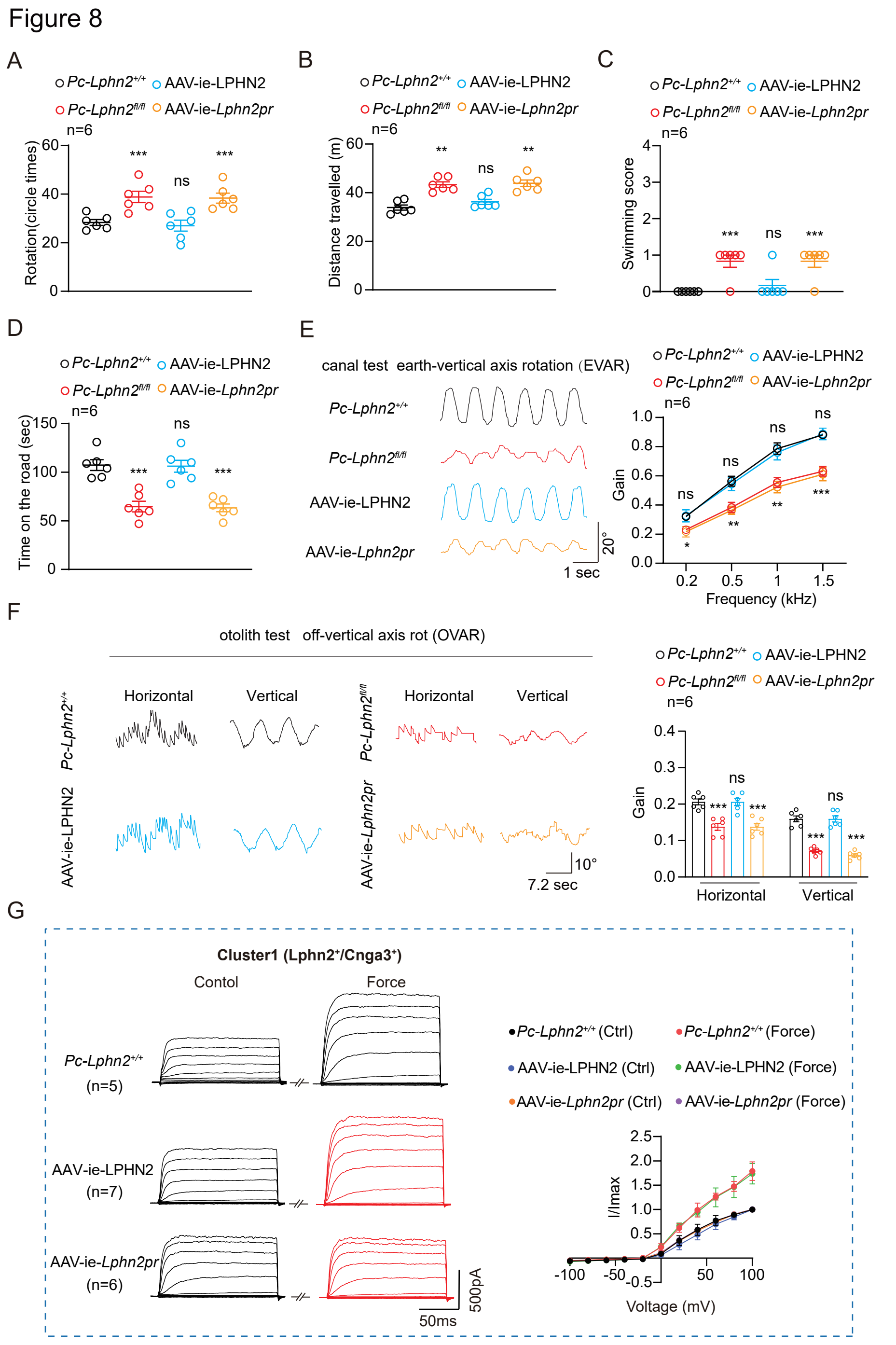
A
Pc-Lphn2+/+
AAV-ie-LPHN2
Pc-Lphn2fl/fl
AAV-ie-Lphn2pr
n=6
Rotation(circle times)
***
ns
***
B
Distance travelled (m)
**
ns
**
C
Swimming score
***
ns
***
D
Time on the road (sec)
***
ns
***
E
canal test earth-vertical axis rotation (EVAR)
Pc-Lphn2+/+
Pc-Lphn2fl/fl
AAV-ie-LPHN2
AAV-ie-Lphn2pr
20°
1 sec
Gain
Frequency (kHz)
F
otolith test off-vertical axis rot (OVAR)
Horizontal
Vertical
10°
7.2 sec
Horizontal
Vertical
G
Cluster1 (Lphn2+/Cnga3+)
Contol
Force
Pc-Lphn2+/+ (n=5)
AAV-ie-LPHN2 (n=7)
AAV-ie-Lphn2pr (n=6)
500pA
50ms
Pc-Lphn2+/+ (Ctrl)
Pc-Lphn2+/+ (Force)
AAV-ie-LPHN2 (Ctrl)
AAV-ie-LPHN2 (Force)
AAV-ie-Lphn2pr (Ctrl)
AAV-ie-Lphn2pr (Force)
I/Imax
Voltage (mV)